Unprecedented radioactive pollution in Spitsbergen's air - first data of the 21st century

Anna Cwanek[1*], Agnieszka Burakowska[2], Ewa Nalichowska[1], Magdalena Długosz-Lisiecka[3], Marek Kubicki[4], Tomasz Wawrzyniak[4], Edyta Łokas[1], Michał Gryziński[2], Gabriela Lubera[1]

[1]Institute of Nuclear Physics, Polish Academy of Sciences, 31-342 Kraków, Poland
[2]National Centre for Nuclear Research, 05-400 Otwock-Świerk, Poland
[3]Lodz University of Technology, Institute of Applied Radiation Chemistry, 90-924 Łódz, Poland
[4]Institute of Geophysics, Polish Academy of Science, 01-452 Warszawa, Poland

Correspondence to: Anna Cwanek (anna.cwanek@ifj.edu.pl)

Abstract. This study focused on the Arctic troposphere, providing an experimental database on nuclear aerosols that has improved considerably since 1999. The activity concentrations of ^{238}Pu, $^{239+240}$Pu and ^{241}Am were determined in surface air at Hornsund, Spitsbergen, between 2007 and 2021. A multivariate approach, incorporating meteorological data, gamma-emitter records and isotopic ratios, was employed to explain transuranium dynamics of changes and provenance. ^{238}Pu and $^{239+240}$Pu levels were comparable to those observed during the last decades at various locations. The highest activity concentrations were 6.61 nBq/m^3 for ^{238}Pu and 15.51 nBq/m^3 for $^{239+240}$Pu, identified in 2015. Although coinciding with the resuspension and atmospheric transport of radionuclides triggered by the 2015 wildfires near the Chernobyl zone, a direct linkage to Hornsund remains uncertain. Further data exploration revealed a correlation between $^{239+240}$Pu and seasonal processes, including local dust redistribution and horizontal tropospheric transport of haze layers from remote areas. While similar mechanisms likely regulated a portion of ^{238}Pu, its random enrichment relative to known nuclear events was frequently noted. As a general pattern, ^{241}Am exhibited particularly elevated activity concentrations, with a maximum of 354 nBq/m^3 detected in 2019. Exceptional signals of ^{237}Np were encountered in 2013, 2014 and 2018. Such contamination was not associated with natural processes; therefore, the possibility of recent radioactive emissions should be considered. Trajectory simulations performed in 2019 indicated prominent transport pathways to Hornsund from northern Eurasia.

1 Introduction

Advances in nuclear science during the 20th century have led to the systematic production of a novel form of environmental contamination on a global scale. Introduced radionuclides, commonly classified as artificial, technogenic, man-made or anthropogenic, were previously non-existent or present in ultra-trace quantities across the Earth system. Although the nuclear era continues today, it has undergone significant changes in scope, objectives and main directions over time. The initial focus on military applications has since evolved toward the development of nuclear power plants, nuclear medicine and all radioactive materials-handling industries. Undoubtedly, the ongoing revolution has brought a plethora of benefits. However,

the parallel identification of new radionuclide emissions and their transport over long distances from the epicentre, with the potential to increase natural background radiation levels, has raised public awareness of the necessity to monitor and control the radiological situation routinely. These measures are required not only for critical groups, objects or areas but also to review the exposures of the population and the surrounding environment at large. Safety standards for radiological protection established by international or intergovernmental organisations such as the International Atomic Energy Agency (IAEA), the Commission of the European Communities (CEC), and the Organisation for Economic Co-operation and Development/Nuclear Energy Agency (OECD/NEA) are based on conceptual frameworks proposed by the International Commission on Radiological Protection (ICRP) (Engelbrecht and Schwaiger, 2008; ICRP, 1991, 2007). Monitoring air radioactivity appears particularly important, given that inhalation represents a significant exposure pathway.

The injection of anthropogenic radionuclides (^{54}Mn, ^{55}Fe, $^{89, 90}$Sr, ^{95}Zr,$^{103, 106}$Ru, ^{125}Sb, ^{131}I, $^{133, 135}$Xe, $^{134, 135, 137}$Cs, $^{141, 144}$Ce, ^{236}U, ^{237}Np, $^{238, 239, 240, 241}$Pu, ^{241}Am, $^{242, 243, 244}$Cm, etc.) into the total environment has been the consequence of a variety of specific events (UNSCEAR, 1982, 2000a), as outlined below:

(a) nuclear explosions and safety tests (> 2300):

• 543 atmospheric nuclear weapon tests (1945−1980) with a legacy of global fallout (GF),

• underwater/underground nuclear weapon tests,

• sub-critical safety trials to burn or explode U and/or Pu without a fission yield,

(b) releases from nuclear reprocessing plants (NRP) and plutonium production plants (PPP), e.g. Sellafield, Cap La Hague, Mayak, Tomsk,

(c) nuclear reactor accidents in nuclear power plants (NPP), e.g. Chernobyl, Fukushima,

(d) satellite, aircraft and submarine accidents, e.g. SNAP 9A, Cosmos 954, Thule, Komsomolets K-278,

(e) effluents associated with radionuclide production for scientific and medical applications,

(f) leaching from dumped nuclear material,

(g) U-mining and tailing,

(h) conventional explosions, including depleted uranium (DU) weapons.

Radioactive debris, once released into the atmosphere, rapidly attaches to ambient aerosols and is subject to the mechanisms that govern air circulation. At least four factors must be given consideration when investigating nuclear particle transport and deposition. Firstly, cooled debris is slowed and eventually halted within the stratosphere by the stability of the air. Subsequent dispersion via eddy diffusion results in their distribution across broad layers and over a wide range of latitudes (Feely et al., 1989; UNSCEAR, 1982). When stratospheric air is carried downward—a process most common at middle latitudes and most rapid during the spring season—residing particles are transported into the upper layers of the troposphere (Feely et al., 1989). The mean residence time of nuclear aerosols reaching the stratosphere has been estimated at approximately 1.5 ± 0.5 years (Hirose and Povinec, 2015). Secondly, the decreased stability of the troposphere during the warmer months increases the rate of vertical transport from the upper troposphere to the middle and lower troposphere (Aegerter et al., 1966). A convective circulation, carrying surface air layers upwards and bringing air from higher layers downwards, is triggered by solar heating.

This is especially pronounced at middle latitudes. However, in the Arctic, the stability of polar air inhibits vertical transport within the troposphere, even during the warmer months (Aegerter et al., 1966). The third key factor concerns the horizontal advection of lower-tropospheric air masses from middle to high latitudes, which peaks during the late winter/early spring seasons. Arriving haze layers in the Arctic are believed to derive from air pollutants emitted in the middle-latitude regions of Asia, Europe and potentially North America (Rahn, 1981). The delivery rates of haze particles have been attributed to a combination of annual fluctuations in the transport regime and changes in pollutant removal (Barrie et al., 1981). The fourth major reason for temporal trends in airborne radioactivity relates to aerosol washout, particularly at sites with large seasonal variation in rainfall amount and frequency (Feely et al., 1989).

It is believed that no significant quantities of artificial radionuclides remain in the stratosphere, as the majority of contaminants derived from past atmospheric emissions (primarily attributable to nuclear weapons testing) had already descended (Hirose et al., 2003; Kierepko et al., 2016). The resuspension phenomenon is considered the dominant mechanism for maintaining residual anthropogenic radioactivity near the surface of the Earth (Hirose and Povinec, 2015). Atmospheric resuspension, a secondary source of contamination, arises from processes such as wind erosion of soil particles, sea spray, flying ash from biomass burning or global desert dust events (Masson et al., 2010, 2021). Additionally, volcanic eruptions have been hypothesised to enhance the transfer of anthropogenic radionuclides from the stratosphere to the troposphere (Alvarado et al., 2014). On the other hand, the recent worldwide releases of ^{131}I and $^{134, 137}$Cs from the Fukushima Daiichi Nuclear Power Plant (FDNPP) accident in 2011 (Koo et al., 2014; Povinec et al., 2013), alongside a 2017 episode of ^{106}Ru in the air over Europe (Bossew et al., 2019), serve as evidence that nuclear incidents may still occur. Continuous measurements of activity concentrations in the atmosphere provide one of the best means of identifying and differentiating between resuspended and freshly released radioisotopes. Moreover, the network of air monitoring stations, when used in conjunction with modelling tools, enables the radioactive plume to be traced back to the point of discharge.

Investigations of nuclear aerosols commenced in the late 1960s and early 1970s. Air radioactivity sampling may be performed for one or more of the following purposes: (a) worker health protection, to ensure that worker exposures are within acceptable limits and As Low As Reasonably Achievable (ALARA); (b) environmental monitoring, to ensure that emissions of contaminants into the environment are within acceptable limits and ALARA; (c) process quality assurance and control, to ensure that all procedures are functioning properly; and (d) emergency preparedness and response, to provide a basis for appropriate action if an incident occurs (Hoover and Maiello, 2010). One of the most extensive and detailed records on atmospheric radioactivity in the world—the Surface Air Sampling Program (SASP)—was conducted by the Environmental Measurements Laboratory (EML) between 1963 and 1999 (Larsen et al., 1995), continuing the work initiated by the Naval Research Laboratory (NRL) during 1957–1962 (U.S. Atomic Energy Commission, U.S. Energy Research and Development Administration, U.S. Department of Energy). SASP's primary objective was to determine the spatial and temporal distribution of specific natural and artificial gamma, beta and alpha emitters (^{7}Be, ^{54}Mn, ^{55}Fe, ^{89}Sr, ^{95}Zr, ^{109}Cd, ^{137}Cs, $^{141, 144}$Ce, ^{210}Pb, $^{238, 239+240}$Pu) in ground-level air at monitoring stations worldwide. In addition to radionuclides of GF origin, the EML programme detected and characterised a post-Chernobyl plume across North America in 1986 (Feely et al., 1988; Larsen et

al., 1989), as well as minute quantities of fission products in Alaska following accidental releases from the Tomsk-7 nuclear complex in 1993 (Larsen, 1994). The implementation of SASP was not limited solely to routine monitoring but also contributed to several scientific observations and discoveries. Notably, the collated database enhanced the trajectory modelling of natural and artificial aerosols through the atmosphere, revealed seasonal cycles of ^{7}Be concentrations in surface air (Feely et al., 1989), or showed the linkage between a decrease in the production rate of cosmogenic radionuclides and an increase in solar activity (Larsen, 1993). Furthermore, the SASP database has been utilised to simulate the global distributions of ^{222}Rn and ^{210}Pb within the EML's three-dimensional transport model (Lee and Feichter, 1995).

Presently, the majority of countries possess nationwide air-monitoring capabilities and participate in internationally coordinated network systems (e.g. CTBTO or Ro5 networks) (Baré et al., 2023; Coyne et al., 2012; Furuno et al., 2024; Steinhauser et al., 2014). Such cooperation facilitates the acquisition of data essential for assessing the radiological situation across vast territories, including even remote Arctic (except for Greenland and the Faroe Islands) and Antarctic regions (AMAP, 2015; Gorzkiewicz et al., 2022). Early-detection stations for atmospheric contamination operate continuously, providing rapid information on selected natural (^{7}Be, ^{22}Na, ^{40}K, ^{210}Pb, etc.) and possible artificial (^{54}Mn, ^{60}Co, ^{95}Zr, $^{103, 106}$Ru, ^{125}Sb, ^{131}I, $^{133, 135}$Xe, $^{134, 137}$Cs, ^{144}Ce, ^{241}Am, etc.) radioisotopes by gamma spectrometry. Some laboratories also employ alpha spectrometry or mass spectrometry to determine $^{238, 239, 240}$Pu and ^{241}Am (artificial actinides) in air filter samples. As a rule, the latter assessment is carried out in the context of a specific nuclear incident, thus encompassing a relatively limited time period (Alvarado et al., 2014; Chamizo et al., 2010; Masson et al., 2010). Longer-term studies are also performed; however, these are less common (Kierepko et al., 2016; Lujaniene et al., 2012; Nalichowska et al., 2023).

In certain regions, no air monitoring programmes dedicated to anthropogenic actinides have been conducted since 2000. This is primarily evident for atmospheric radioactivity in the Arctic, where data on levels, isotopic signatures, or temporal variations of $^{238, 239, 240}$Pu and ^{241}Am are lacking in the 21st century. For several reasons, research in this domain remains of particular interest and importance. The artificial actinides have attained tracer status in investigations of atmospheric circulation or natural 'feeder' mechanisms through which previously deposited contaminants are transferred back to the air (Alvarado et al., 2014; Hirose et al., 2003; Hirose and Povinec, 2015; Masson et al., 2010). $^{238, 239, 240}$Pu and ^{241}Am are recognised ~~as~~ among the most radiotoxic elements that may be directly inhaled with aerosols or accumulate in plants and animals. Also noteworthy are the relatively long half-lives of these radionuclides ($^{238, 239, 240}$Pu: $T_{1/2}$ = 87.7 years, 2.41 10^{4} years, 6.56 10^{3} years, respectively; ^{241}Am: $T_{1/2}$ = 432.6 years), implying that such pollution will persist in the environment over multiple generations. In the context of potential terrorist attacks involving 'dirty bomb', undeclared nuclear activity, and any intentional or unintentional releases from nuclear installations, the development of novel monitoring strategies seems imperative (Mietelski and Povinec, 2020). Specifically, the world's national and international nuclear safety monitoring networks should incorporate routine measurements of pure beta and alpha emitters in the atmosphere.

The research project outlined in this paper aimed to address limitations in database capabilities and to enhance understanding of the processes governing artificial actinides suspended in the ground-level air layers of Hornsund, SW Spitsbergen, between 2007 and 2021. The following key objectives were set and subsequently achieved:

(a) determination of activity concentrations of ^{238}Pu, $^{239+240}$Pu and ^{241}Am,

(b) evaluation of mutual correlations between ^{238}Pu, $^{239+240}$Pu, ^{241}Am and ^{7}Be, ^{137}Cs, ^{210}Pb, suspended dust and selected meteorological factors,

(c) analysis of seasonality and long-term trends in time-series data for ^{238}Pu, $^{239+240}$Pu and ^{241}Am,

(d) estimation of ^{238}Pu/$^{239+240}$Pu and ^{241}Am/$^{239+240}$Pu activity ratios,

(e) modelling of air trajectories in the event of unusual nuclear signals being detected.

2 Materials and methods

2.1 Study area and sampling

Long-term observations of atmospheric radioactivity in the Arctic are a central component of the Arctic Monitoring and Assessment Programme (AMAP) (AMAP, 2002, 2009, 2015). The geographical locations of air filter stations across the northern regions, including Iceland, the Canadian Arctic, northern Finland, Sweden and Norway, as well as the Svalbard archipelago, are mapped in Fig. 1b. To the best of our knowledge, no coordinates are publicly available for nuclear aerosol samplers placed within the Russian Arctic (AMAP, 2009, 2015). Consequently, these stations are not shown on the map.

Air monitoring of radioisotopes is carried out at the Stanisław Siedlecki Polish Polar Station (77°00′ N, 15°33′ E, 10 m a.s.l.), one of the few permanently operating units north of the Arctic Circle (Burakowska et al., 2021) (Fig. 1d). The Polish Polar Station, located 300 m from the shore of Isbjørnhamna Bay in the Hornsund fjord of SW Spitsbergen, Svalbard archipelago (Fig. 1a, 1c), was established during the International Geophysical Year in 1957. Over decades, the site has evolved into a modern interdisciplinary scientific platform conducting research projects to better understand the functioning of the Arctic environment and the changes it undergoes (Wawrzyniak and Osuch, 2020).

A high-performance air intake system for the AZA-1000 model was launched at Hornsund in 2002 to enable continuous operation at low temperatures (Burakowska et al., 2021). Aerosols are collected on Petrianov FPP-15-1.5 filters—post-chlorinated polyvinylchloride (CPVC) fibre—with a high retention capacity for particles of diameter not less than 0.3 μm. The filter efficiency for aerosols with diameters between 0.3 and 1.25 μm, at linear air velocities through the filter from 0.25 to 0.4 m/s, reaches 96−99% (Kierepko et al., 2016). The high airflow (approximately 450 m^3/h) ensures the collection of a representative proportion of aerosols in a single air filter sampled over 1 week from approximately 50,000–100,000 m^3 of pumped air. This research scope spanned 2007 to 2021, including the 2011−2013 gap in data collection, during which a considerable number of weekly filters were not available.

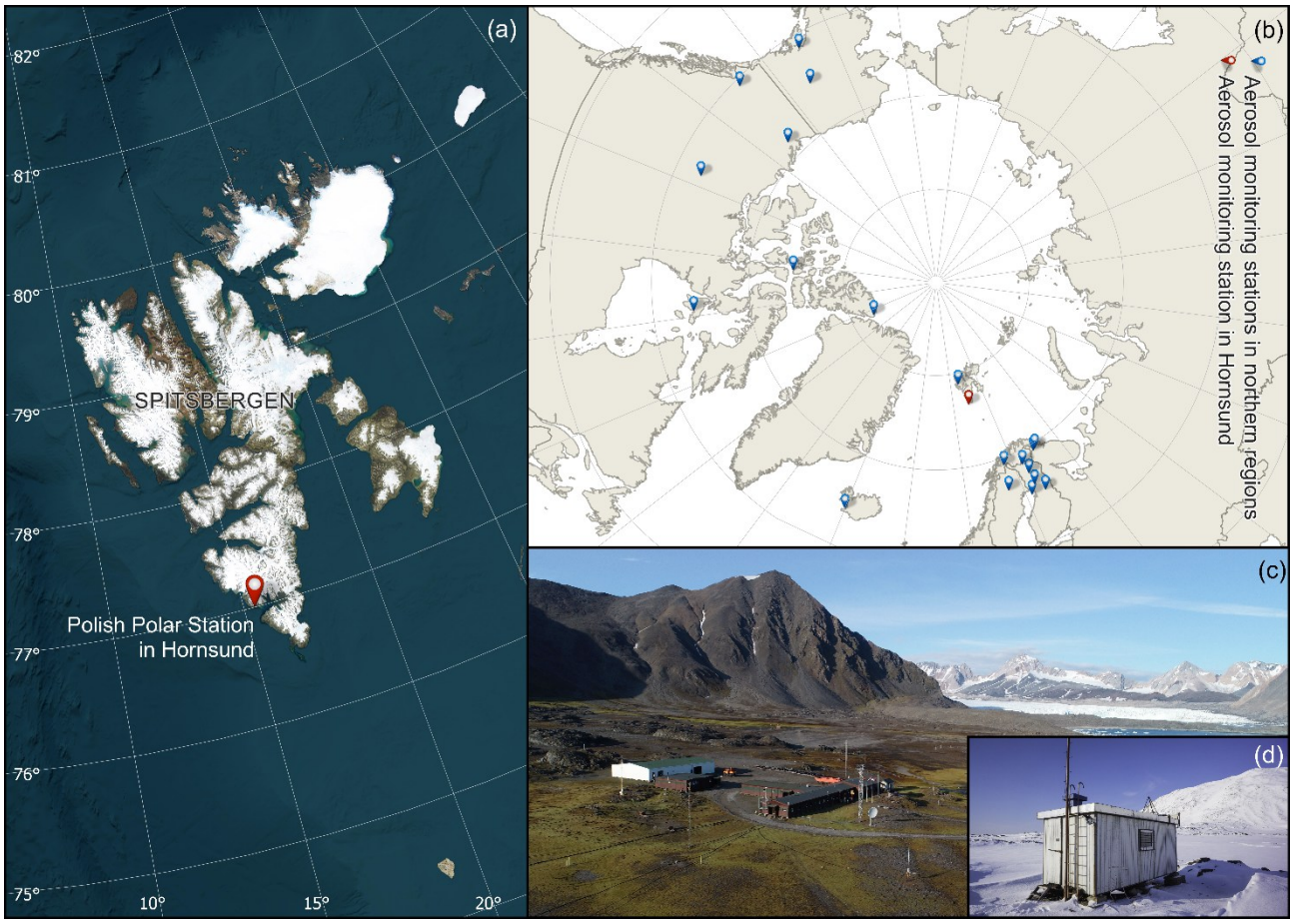

Figure 1: Map of Spitsbergen showing the location of the Stanisław Siedlecki Polish Polar Station at Hornsund (a), the mapped sites for aerosol sampling in the northern regions (b), the facilities of the Stanisław Siedlecki Polish Polar Station (c), and the building housing the AZA-1000 air sampling system at the Stanisław Siedlecki Polish Polar Station (d). The red pin marks the Stanisław Siedlecki Polish Polar Station, and the blue pins mark other stations. Basemap source: Esri, Maxar, Earthstar Geographics, and the GIS User Community. Photographs by T. Wawrzyniak.

2.2 Meteorological data

Since July 1978, systematic, continuous measurements and observations have been conducted at the Hornsund meteorological site (indexed by the international numbering system 01003; https://oscar.wmo.int/surface/) at World Meteorological Organisation (WMO) standards (Wawrzyniak and Osuch, 2020). A detailed description of the measurements and instruments was provided in a collective work edited by Marsz and Styszyńska (2013) while selected information on meteorological variables and current sensors is presented in Table S1.

The Svalbard archipelago experiences the highest air temperatures at these latitudes, and the observed climate changes are the most pronounced on Earth (IPCC, 2019). Analysis of the climatological dataset covering 40 years (1978–2018) provides a comprehensive overview of the meteorological conditions in the Hornsund region (Wawrzyniak and Osuch, 2020). The mean annual air temperature is -3.7 °C. The coldest month is March, with a mean air temperature of -10.2 °C, and the warmest month is July, with a mean air temperature of 4.6 °C. The West Spitsbergen Current contributes to a relatively moist climate, as evidenced by a mean annual precipitation of 478 mm. However, the interior of Spitsbergen is much drier (200 mm). Winds blowing from the east along the Hornsund fjord are prevailing, and the wind speed regime shows lower average values in summer months (minimum 4.0 m/s in June) but higher average values in winter months (maximum 7.1 m/s in February). Such variability results from extreme cyclone activity that often occur during Arctic winters (Rinke et al., 2017). The polar night lasts 104 days (31 October–11 February), while the polar day lasts 117 days (24 April–18 August).

This assessment encompassed daily data on air temperature (°C), sum of precipitation (mm), atmospheric pressure (hPa), relative humidity (%), cloudiness (octa), visibility (marine scale), sunshine duration (h), wind speed (m/s) and wind direction (°), collected between 2007 and 2021. For most meteorological parameters, daily mean values were derived from 3-hourly values (eight values per day, between 00:00 and 21:00 UTC). For precipitation, 6-hourly values (12:00, 18:00, and 00:00, 06:00 UTC of the following day) were used, whereas the daily sum of solar radiation from the Campbell–Stokes recorder was obtained at midnight (Wawrzyniak and Osuch, 2020). The wind rose, changes in mean air temperature and sum of precipitation, determined daily at Hornsund for 2007–2021, are depicted in Fig. 2a, 2c and 2d.

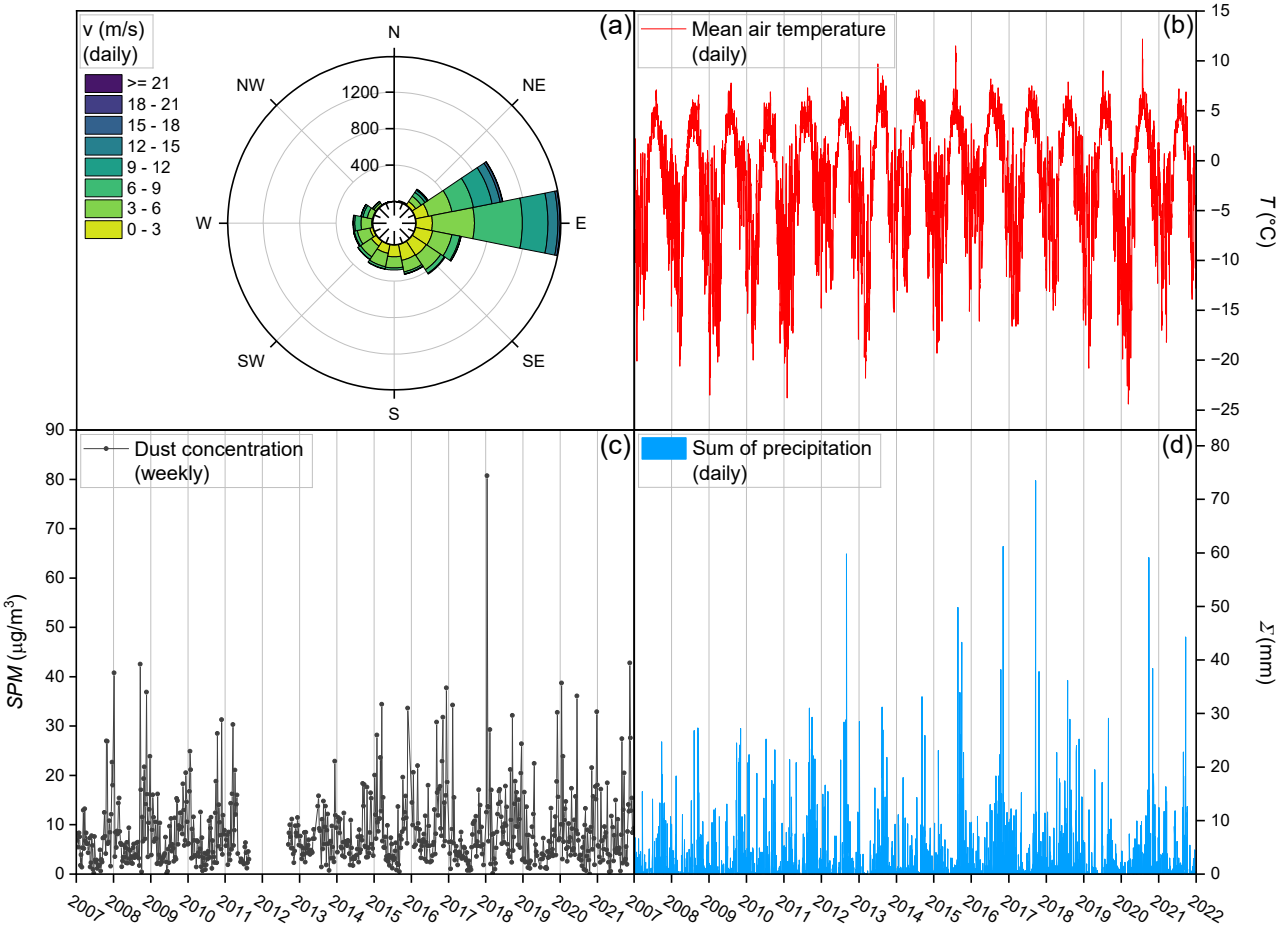

Figure 2: Wind rose according to wind speed (*v*) and wind direction (N, NE, E, SE, S, SW, W, NW) (a), together with the variability of mean air temperature (*T*) (b), dust concentration (*SPM*) (c), and sum of precipitation (*Σ*) (d), measured at Hornsund during 2007–2021.

2.3 Gamma spectrometry measurements

A set of weekly air filters was supplied from the Polish Polar Station in Hornsund, Svalbard archipelago, to the National Centre for Nuclear Research (NCBJ) in Świerk, Poland. Before measurement, each sample was desiccated using halogen infrared heaters (500 W, 220–230 V) to determine the dry mass of the collected dust. Following this, the suspended particulate matter concentration (*SPM*, μg/m^3) was estimated at weekly intervals (Fig. 2b). Lastly, all filters were compressed individually to a diameter of 4.5 cm and a thickness of ca. 5 mm. Gamma-ray spectra were measured using a Canberra set, comprising HPGe detectors positioned inside low-background shielding chambers with 10 cm-thick lead walls. Detector efficiencies range from 35 to 45%, and the energy resolutions are 1.9–2.0 keV for 1.33 MeV photons from ^{60}Co. Spectrometer calibration is performed

utilising a certified source with well-known radioisotope activities. Data acquisition is facilitated by the Genie-2000 software (Mirion Technologies). Correction factors were applied to all results to account for decay during sampling, decay from the end of sampling to the start of measurement, and decay during measurement. The self-absorption correction was found to be negligible due to the samples' low height. The minimum measurable activity concentration for gamma spectrometry (MDC_γ, $\mu Bq/m^3$) was calculated according to the Currie law (Currie, 1968). Values of MDC_γ ranged from 0.1–1.0 $\mu Bq/m^3$, depending on the radionuclide. The present study incorporated weekly results on the volume activities (C, $\mu Bq/m^3$) of ^{7}Be, ^{137}Cs and ^{210}Pb, arranged into time series spanning from 2007 to 2021.

2.4 Radiochemical procedures and alpha spectrometry measurements

The primary phase of the analysis determined the activity concentrations of ^{238}Pu, $^{239+240}Pu$ and ^{241}Am by alpha spectrometry. Given the presumed low quantities of artificial alpha emitters in the Hornsund atmosphere over the last two decades, it was hypothesised that the weekly aerosol sample would yield ^{238}Pu, $^{239+240}Pu$ and ^{241}Am levels below the minimum measurable activity concentrations for alpha spectrometry (MDC_α, nBq/m^3). A similar conclusion has been drawn by researchers investigating anthropogenic radioisotopes in the ground-level air of European cities during the 21st century (Kierepko et al., 2016; Lujaniene et al., 2012; Nalichowska et al., 2023). Therefore, a set of weekly air filters from Hornsund was combined, corresponding approximately to one-quarter of a year, for the 2007−2010 and 2014−2021 intervals. Due to incomplete collection of weekly air filters from 2011 to 2013, only one biennial sample was prepared for 2011–2012, while two half-yearly samples were obtained in 2013. The aggregate samples generally comprised 9–14 weekly air filters, with associated total air volumes ranging from 630,000 to 996,319 m^3.

The radiochemical separation of analytes from matrix components (such as organic matter, aeolian dust, anthropogenic particles or filter material) followed the general outline of the method by La Rosa and co-workers in the IAEA Laboratories at Seibersdorf (La Rosa et al., 1992), as well as procedure implemented at the Institute of Nuclear Physics, Polish Academy of Sciences (IFJ PAN) (Mietelski et al., 2000, 2008), which had previously been tested in air filter investigations (Kierepko et al., 2016; Nalichowska et al., 2023). All non-concentrated reagents were prepared by dilution with ultrapure deionised water (Milli-Q®, 18.2 MΩ cm; Merck KGaA). Sample treatment began with incineration at 600 °C in a muffle furnace. Next, internal tracers of ^{242}Pu (ca. 0.0041 Bq per sample) and ^{243}Am (ca. 0.0077 Bq per sample) were dosed (SRM 4334j and SRM 4332e, respectively; NIST). Near-complete sample mineralisation was achieved using concentrated acids (HF, HNO_3, HCl and H_3BO_3), yielding a filtered 1M HNO_3 solution. The plutonium fraction was separated from the 8M HNO_3 feed solution via anion exchange with AmberChrom™ 1x8 resin (100–200 mesh; Sigma-Aldrich), preceded by adjustment of the Pu(IV) oxidation state. Given thorium's ability to adsorb onto the resin bed, its elution was performed before plutonium elution to prevent interference between plutonium and thorium isotopes during alpha-spectrum acquisition. Pu(IV) was washed out of the resin bed by passing through a mixture of 0.1M HF-0.1M HCl. The americium analyte, significant quantities of lead, possible traces of thorium, rare-earth elements (REE), and other matrix impurities were expected to be present in the main effluent (8M HNO_3). Experience has shown that purification steps are necessary for effective extraction and measurement of

the americium fraction. The initial removal of lead was achieved by retention on SR resin (100–150 μm particle size; Triskem International) from an 8M HNO_3 solution. The alkali metals, alkaline earth metals and anionic components were eliminated by subsequent co-precipitation of these elements with calcium oxalate at pH ~ 2.5 and with iron hydroxide(III) at pH ~ 9. Repurification from any residual traces of thorium was then performed using TEVA resin (100–150 μm particle size; Triskem International). The Am(III) was separated from the REE by anion-exchange chromatography on AmberChrom™ 1x8 resin (100–200 mesh; Sigma-Aldrich) in a methanol-acid medium. Isolated isotopes of Pu and Am were co-precipitated from aqueous solutions with NdF_3 and deposited onto Resolve® filters (Triskem International).

Separation of the interfering analytes ^{237}Np and ^{242}Pu in a few alpha sources proved essential for further assessment. Thus, a simplified version of the procedure by La Rosa et al. (2005) was used. In the initial stage, the Pu+Np alpha sources were wet-digested with concentrated acids (H_3BO_3, HCl, $HClO_4$ and HNO_3) and then adjusted to the required oxidation state (IV). Plutonium and neptunium were separated by column chromatography utilising an AmberChrom™ 1x8 resin (100–200 mesh; Sigma-Aldrich). The 8M HNO_3 feed solution was passed through the column, resulting in strong retention of Np(IV) and Pu(IV). After the 8M HNO_3 column rinse, the receiver was converted from the nitrate to the chloride form with 10M HCl. Pu(III), reduced from Pu(IV), was selectively eluted with 0.1M NH_4I-9M HCl, whereas Np(IV) was washed out by a mixture of 0.1M HF-0.1M HCl. The Pu and Np alpha sources were re-prepared by co-precipitation with NdF_3.

For data acquisition, alpha sources were placed adjacent to passivated implanted planar silicon detectors (PIPS®, Mirion Technologies) in the vacuum chambers of the AlphaAnalyst™ 7200 spectrometer (Mirion Technologies). The PIPS® detector, with a 450 mm^2 active area, has an efficiency of approximately 40% and an energy resolution of 18 keV for 5.486 MeV alpha particles from ^{241}Am. All alpha spectra were processed in OriginPro® 2024b (OriginLab Corporation), using the Peak Analyser tools for baseline correction, peak detection, integration or fitting. The latter option was applied to resolve overlapping spectral lines by fitting bigaussian curves. Following the Currie law (Currie 1968), MDC_α values were typically 0.06−0.3 nBq/m^3 for $^{238,\ 239+240}$Pu and ^{241}Am. The mean recoveries of the Pu and Am fractions after the chemical procedure were calculated as 80.7 ± 2.5% and 43.5 ± 2.2%, respectively. The dataset comprised activity concentrations (C, nBq/m^3) of ^{237}Np, $^{238,\ 239+240}$Pu and ^{241}Am, largely determined in quarters between 2007 and 2021.

2.5 Statistical analysis and modelling

For each radioisotope except ^{237}Np, the basic descriptive statistics were computed according to the time intervals at which the radioisotopes were measured. These included the minimum (min), 25th percentile (*Q1*), median, 75th percentile (*Q3*), maximum (max), interquartile range (*IQR*), mean, and standard deviation (*SD*). To spot outliers in the dataset, Tukey's interquartile range method with multiplier $k = 3$ was employed (Hoaglin 2003). Meteorological indicators, the *SPM* factor and gamma emitters were treated as supporting variables to facilitate a thorough evaluation of the annual dynamics of artificial actinides in the surface air. Consequently, the next stages of statistical analysis required converting daily and weekly parameters into quarterly representations. Data aggregation was performed using the following mathematical operations:

(a) arithmetic mean for daily air temperature, atmospheric pressure, visibility, relative humidity and cloudiness,

(b) sum for daily precipitation and sunshine duration,

(c) magnitude of the resultant wind velocity vector for each of the eight sectors (W, E, N, S, NW, NE, SE, SW), based on daily wind direction and speed,

(d) sum of weekly activities or masses divided by the associated volume of pumped air in a specific quarter for gamma emitters and *SPM*, respectively.

The input database for calculating Spearman's correlation coefficient (R) was constructed by eliminating outliers in radioisotope activity concentrations. Given the non-quarterly nature of the data, the 2011–2013 interval was omitted from the correlation matrix for alpha emitters against all other variables. The correlation was considered statistically significant at a probability level less than or equal to 0.05 ($p \leq 0.05$). Data analysis and visualisation were performed in Python using the following libraries: NumPy, pandas, matplotlib, SciPy and seaborn.

To reconstruct radionuclide fate across the explored Arctic region, three-dimensional air-mass trajectories were simulated using the Hybrid Single-Particle Lagrangian Integrated Trajectory (HYSPLIT) model developed by the National Oceanic and Atmospheric Administration (NOAA, U.S. Department of Commerce). The system offers a range of applications in the domain of propagation and dispersion modelling of forest smoke, hazardous materials, chemicals, and radioactive materials, including the decay of radionuclides in gaseous or particulate forms (Stein et al., 2015). Backward simulations were performed for a final position at 77°00′ N, 15°33′ E (Hornsund), whereas a forward trajectory was generated from an initial position at 72°55′ N, 54°01′ E (Novaya Zemlya). All trajectories were reconstructed using archived meteorological data from the Climate Data Centre (CDC) and the Global Data Assimilation System (GDAS) repositories, both accessed via the NOAA Air Resources Laboratory (ARL) server.

3 Results and discussion

3.1 Descriptive statistics and time series

This study examined radioisotopes divided into two categories, here referred to as 'target' and 'background'. The first group comprised subject analytes (^{238}Pu, $^{239+240}$Pu, ^{241}Am), whereas the second group, mostly reported by Burakowska et al. (2021), provided supplementary information (^{7}Be, ^{137}Cs, ^{210}Pb). Table 1 summarises the descriptive statistics for both groups. As expected, naturally occurring radionuclides (^{7}Be, ^{210}Pb) suspended in the lower atmosphere of Hornsund reached higher activity concentrations than the artificial ones (^{137}Cs, ^{238}Pu, $^{239+240}$Pu, ^{241}Am). The mean and median values exhibited significant dispersion for each radionuclide, reflected by elevated standard deviations and interquartile ranges (Table 1). Estimating upper limits for outliers (> *Q3 + 3*IQR*) was a pivotal phase in the assessment. All outlier points were highlighted in the time-series graphs (Fig. 3 and 4) and treated as potential radiological episodes. Outcome data have been further plotted as combined violin and strip graphs, demonstrating non-normal probability density distributions for ^{7}Be, ^{137}Cs, ^{210}Pb, ^{238}Pu, $^{239+240}$Pu and ^{241}Am (Fig. 5). Since the strip plot arranges points along the x-axis to minimise overlap, some points extend beyond the x-axis range of the violin plot (by default, Seaborn adds random jitter to the positioning of the points; https://seaborn.pydata.org/).

Table 1: Descriptive statistics for alpha- and gamma-emitters measured in aerosol samples collected at Hornsund between 2007 and 2021 (input dataset is available at https://doi.org/10.48733/no6.25.015).

	mean	*SD*	min	*Q1*	median	*Q3*	max	*IQR*	*Q3 + 3*IQR*
^{7}Be (µBq/m^3)	2022	1149	188	1177	1853	2642	8378	1465	7037
^{137}Cs (µBq/m^3)	3.54	28.17	0.07	0.17	0.26	0.45	344.76	0.28	1.28
^{210}Pb (µBq/m^3)	255	249	10	87	163	338	1649	251	1091
$^{239+240}$Pu (nBq/m^3)	1.42	2.55	0.23	0.47	0.77	0.97	15.51	0.50	2.48
^{238}Pu (nBq/m^3)	0.72	1.38	0.02	0.09	0.21	0.59	6.61	0.50	2.09
^{241}Am (nBq/m^3)	31.4	53.3	2.6	11.3	14.9	33.4	353.6	22.1	99.8

3.1.1 Background radioisotopes

Cosmogenic ^{7}Be ($T_{1/2}$ = 53.22 days) is produced through spallation of light atomic nuclei (carbon, nitrogen and oxygen) by primary (protons) and secondary (neutrons) particles (Beer et al., 2019). Gaggeler (1995) reported that approximately 67% of ^{7}Be is produced in the stratosphere, with the remaining 33% in the troposphere. ^{7}Be maxima are regularly observed in late spring (2nd/3rd quarters) in ground-level air layers at mid-latitudes, coinciding with intensive exchange between the stratosphere and the troposphere and subsequent vertical transport within the troposphere (Błażej and Mietelski, 2014; Dueñas et al., 2001; Grossi et al., 2016; Kulan et al., 2006). In contrast, atmospheric investigations at Hornsund (Burakowska et al., 2021) revealed a ^{7}Be activity concentration peaks in late winter/early spring (1st/2nd quarters), as depicted in Fig. 3. Reduced vertical mixing of air masses in polar regions leads to lower ^{7}Be levels in late spring compared with temperate zones. Therefore, the seasonal fluctuations of ^{7}Be at Hornsund were considered primarily governed by horizontal tropospheric transfer of haze layers from Eurasian regions that reached higher latitudes during late winter and early spring. Another process that may have contributed to the ^{7}Be variation at Hornsund was wet scavenging, in which aerosols are washed out of the atmosphere and deposited on Earth's surface. Long-term data analysis also confirmed the relationship between the ^{7}Be air concentration and the 11-year solar activity cycle. The intensity of cosmic radiation has been shown to decrease with increasing solar activity (Beer et al., 2019). Hence, the atmospheric production of ^{7}Be is inversely proportional to the sunspot number. During 2002–2017, explored by Burakowska et al. (2021), the lowest sunspot number per week occurred in 2009–2010, which most likely accounted for ^{7}Be outlier values > 7037 µBq/m^3 identified at Hornsund in 2010 (Table 1, Fig. 3).

^{210}Pb ($T_{1/2}$ = 22.3 years) is a radionuclide of terrestrial origin and a member of the uranium-radium series. Its presence in the atmosphere is associated with the decay of ^{222}Rn ($T_{1/2}$ = 3.8 days), which has previously been exhaled from the Earth's surface into the atmosphere (Gäggeler, 1995). Grossi et al. (2016) noted that although the ^{210}Pb concentration can increase with altitude and reach high values in the stratosphere over large continental areas, it accumulates mainly in the troposphere. The majority of ^{210}Pb is present in accumulation-mode aerosol particles, which are primarily removed from the atmosphere by precipitation. Despite different origins, the behaviour of ^{210}Pb and ^{7}Be in the lower atmosphere was found to be similar at Hornsund, where

the annual fluctuation of ^{210}Pb was only slightly shifted relative to that of ^{7}Be. Namely, elevated activity concentrations of ^{210}Pb were identified in late winter (1st quarter) (Fig. 3). These observations aligned with ^{210}Pb results from Ny-Ålesund, Spitsbergen (Paatero et al., 2003, 2010). The ^{210}Pb variations at Hornsund were predominantly influenced by climate patterns and the inflow of air masses, possibly continental, from the northern part of Asia or Europe. Outlier values of ^{210}Pb exceeding 1091 μBq/m^3 were noticed in 2008, 2009, 2010, 2015, 2019 and 2020 (Table 1, Fig. 3), which corresponded to a reduced sum of precipitation in the listed years (Fig. 2d).

An analysis of fission-produced ^{137}Cs ($T_{1/2}$ = 30.07 years) in ground-level air layers at Hornsund over 2007−2021 revealed a median of 0.26 μBq/m^3 (Table 1). A distinct increase in activity concentration, reaching approximately 350 μBq/m^3, was detected in 2011 (Fig. 3). Elevated ^{137}Cs results—persisting in the atmosphere for approximately nine weeks—were linked to the FDNPP failure (AMAP, 2015; Burakowska et al., 2021). This accident was identified as the primary source of outlier values (Table 1, Fig. 3). Additional outliers appeared in 2015 and 2016, but to a far lesser extent (Fig. 3). ^{137}Cs activity concentrations at Hornsund generally fell within the range of approximately 0.05–1.50 μBq/m^3 established by international air monitoring at 17 stations covering most of the Arctic region during 2013−2020 (Zhang et al., 2022). Interestingly, a clear seasonal pattern was noticed for Yellowknife (62°29′ N, 114°28′ W), where higher levels of ^{137}Cs in the summer tightly matched the occurrence of fire plumes at the station location (Zhang et al., 2022). These findings implied that ^{137}Cs deposited worldwide after past nuclear events can be reinjected into the atmosphere on a large scale through combustion and then transported over long distances. In contrast, randomly observed lower ^{137}Cs signals (< 3 μBq/m^3) may be due to local resuspension of soil in summer or dust in winter.

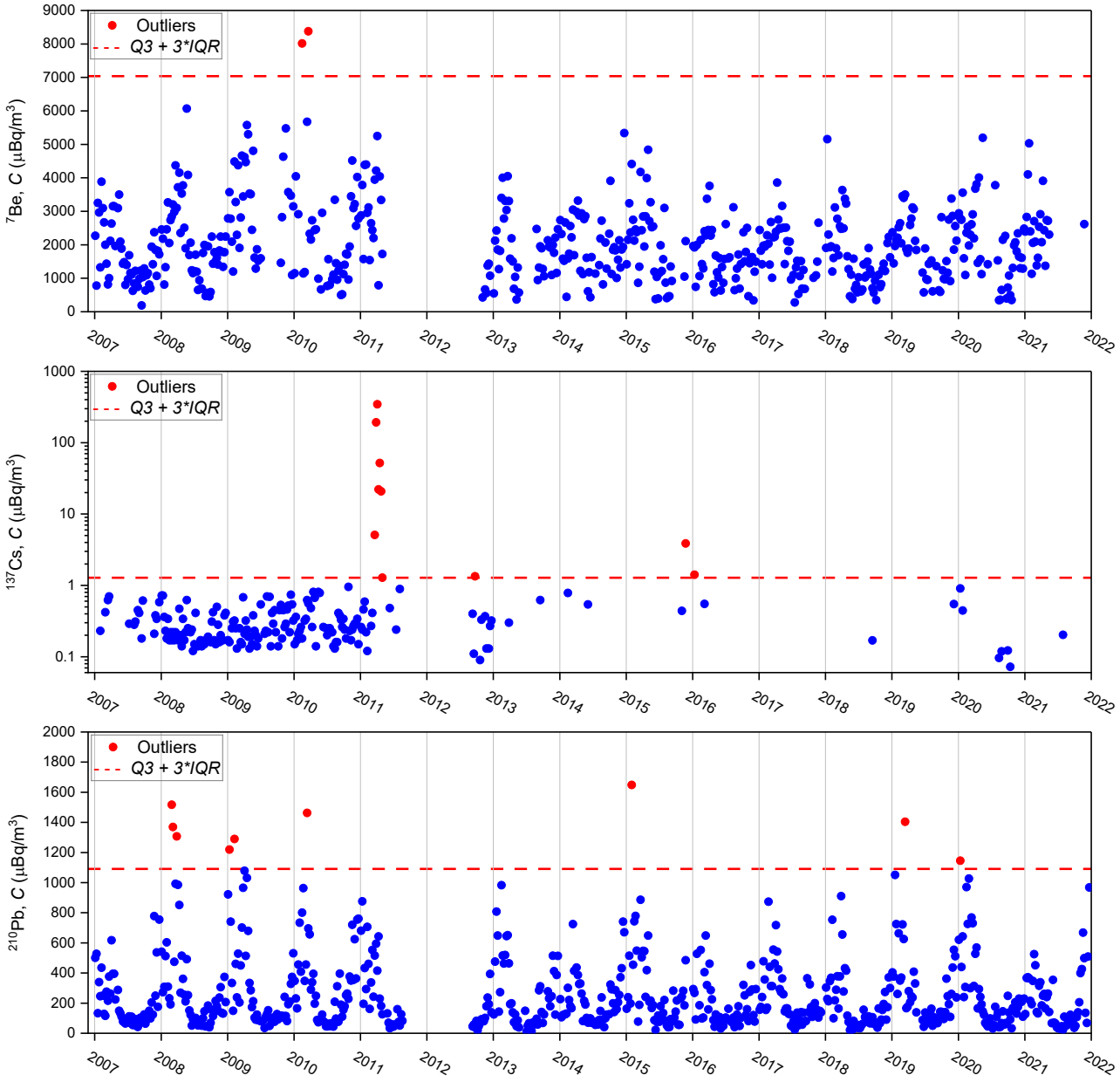

345 **Figure 3: Time series of ^{7}Be, ^{137}Cs and ^{210}Pb activity concentrations (*C*) in weekly air filters sampled at Hornsund during 2007–2021. Blue dots indicate non-outlier values, and red dots indicate outlier values.**

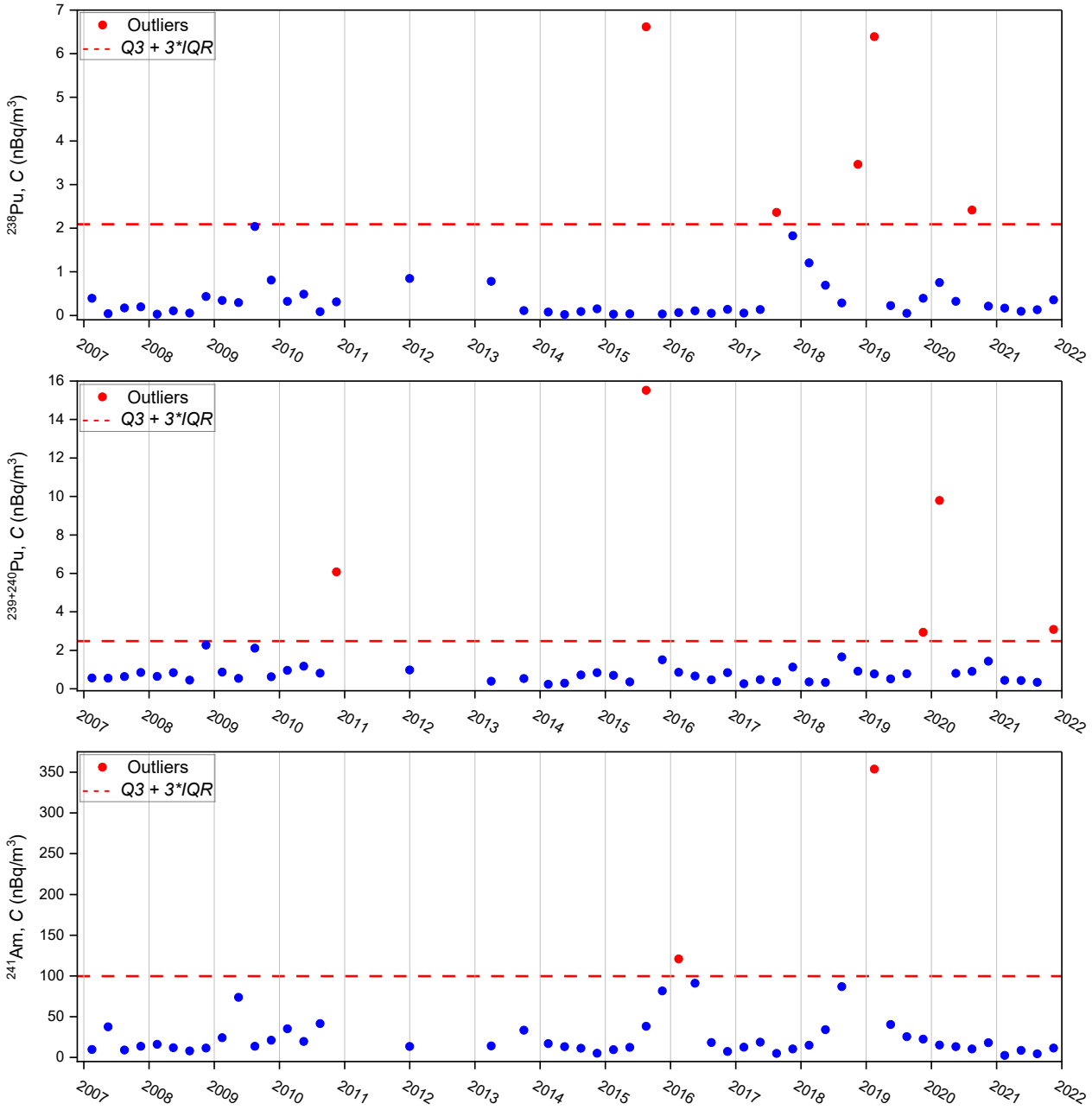

Figure 4: Time series of ^{238}Pu, $^{239+240}$Pu and ^{241}Am activity concentrations (*C*) in quarterly air filters sampled at Hornsund during 2007–2021. Blue dots indicate non-outlier values, and red dots indicate outlier values.

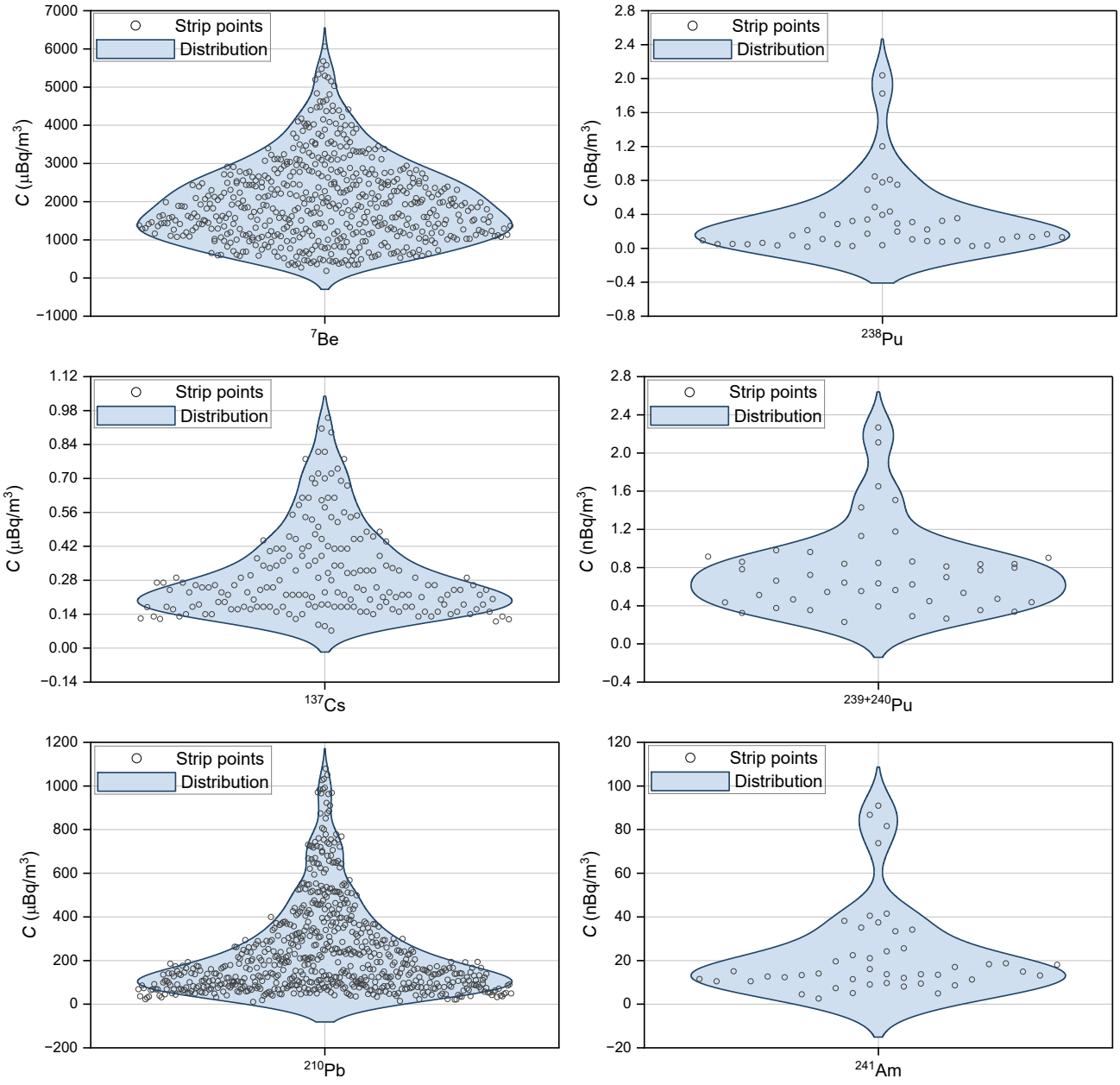

350

Figure 5: Combined violin and strip plots for ^{7}Be, ^{137}Cs, ^{210}Pb, ^{238}Pu, $^{239+240}$Pu and ^{241}Am activity concentrations (*C*) in weekly or quarterly aerosol samples collected at Hornsund between 2007 and 2021.

3.1.2 Target radioisotopes

Time-series analysis for artificial alpha emitters of ^{238}Pu, $^{239+240}$Pu and ^{241}Am suspended in Hornsund air between 2007 and 2021 did not reveal any clear annual fluctuations (Fig. 4). The highest activity concentrations were 6.61 nBq/m^3 for ^{238}Pu and 15.51 nBq/m^3 for $^{239+240}$Pu, both in the 3rd quarter of 2015, whereas the maximum for ^{241}Am was 353.6 nBq/m^3 in the 1st quarter of 2019 (Fig. 4). Additional peaks were noted in the following years: 2017, 2018, 2019 and 2020 for ^{238}Pu; 2010, 2019, 2020 and 2021 for $^{239+240}$Pu; and 2016 for ^{241}Am (Fig. 4). These elevated activity concentrations were classified as outliers (Table 1). Examples of alpha spectra representing outliers of $^{238, 239+240}$Pu in 2015 and ^{241}Am in 2016 are depicted in Fig. S1. The median values (Table 1) of ^{238}Pu and $^{239+240}$Pu (0.21 nBq/m^3 and 0.77 nBq/m^3, respectively) were approximately two or three orders of magnitude lower than those of ^{241}Am and ^{137}Cs (14.9 nBq/m^3 and 260 nBq/m^3, respectively). The distinct enhancement of ^{137}Cs relative to $^{239+240}$Pu and ^{238}Pu was expected, given that past nuclear events had released at least a tenfold higher activity of ^{137}Cs than $^{239+240}$Pu, ^{241}Am or ^{238}Pu (UNSCEAR, 1993, 2000a,b). However, a particular challenge arose in explaining why the median of ^{241}Am was notably higher than that of $^{239+240}$Pu. Potential reasons for the observed dynamics of changes and isotopic compositions of artificial actinides in the lower atmosphere of Hornsund for 2007–2021 required further analysis, to be discussed in the following sections.

Signals of plutonium and americium isotopes were found at other aerosol sampling sites during the 21st century. Nalichowska et al. (2023) studied temporal variations of ^{238}Pu and $^{239+240}$Pu in monthly air filters between 2010 and 2016 in Kraków, Poland (50°04′ N, 19°58′ W). The activity concentrations measured in Kraków averaged 2.07 nBq/m^3 for $^{239+240}$Pu and 0.15 nBq/m^3 for ^{238}Pu, corresponding to the mean values obtained at Hornsund (Table 1). Moreover, the highest activity concentrations of 1.27 nBq/m^3 for ^{238}Pu and 13.1 nBq/m^3 for $^{239+240}$Pu were detected in the 1st and 3rd quarters of 2015, respectively. Investigations of monthly aerosol samples collected in Vilnius, Lithuania (54°42′ N, 25°30′ E) demonstrated a 0.9–300 nBq/m^3 range of $^{239+240}$Pu, with a mean activity concentration of 13.4 nBq/m^3 for the 1995–2011 period. ^{241}Am results varied there from 0.32 to 25 nBq/m^3, reaching an average of 4.3 nBq/m^3 for the shorter 2005–2006 interval (Lujaniene et al., 2012). This implied an order-of-magnitude higher and order-of-magnitude lower levels than those established at Hornsund for $^{239+240}$Pu and ^{241}Am, respectively (Table 1). The Preila air sampling station (55°20′ N, 21°00′ E), situated 300 km from Vilnius, recorded a $^{239+240}$Pu range of 1−16 nBq/m^3, averaging 6.2 nBq/m^3, in 1995−1999 (Lujaniene et al., 2012). The disparities between the Preila and Vilnius datasets were attributed to the sampling conditions. The Preila station is situated at the Curonian Split on the seashore, where prevailing winds from the Baltic Sea are expected to result in reduced radionuclide contributions from soil resuspension and the Chernobyl-contaminated zone compared to the Vilnius station (Lujaniene et al., 2012). Furthermore, a recent study of the urban air in Lodz, Poland (51°48′ N, 19°30′ E) identified ^{241}Am signals of 305–4241 nBq/m^3 in weekly aerosol filters from April to June 2021 (Długosz-Lisiecka and Isajenko, 2024). During the same period, a decrease in the activity concentration of ^{241}Am to several nBq/m^3 was noticed in surface air at Hornsund.

Data on ^{238}Pu, $^{239+240}$Pu and ^{241}Am in the lower atmosphere for the most northerly areas during the 21st century are generally unavailable. The primary focus of the research sites mapped in Fig. 2b is on ^{7}Be, ^{133}Xe, ^{137}Cs and ^{210}Pb (+ ^{90}Sr, controlled at

sites in northern Russia; not marked in Fig. 2b) (AMAP, 2002, 2009, 2015). The present investigation, therefore, constitutes the sole radioactivity-monitoring effort to have yielded long-term results on artificial actinides in the Arctic atmosphere over the past two decades. The earlier assessment, encompassing stations proximate to and above the Arctic Circle, was carried out by the NRL between 1957 and 1962, followed by the EML SASP continuation from 1963 to 1999 (Larsen et al. 1995). The time series of ^{137}Cs and $^{239+240}$Pu based on data from stations north of 50° N (Kap Tobin, Constable Point, Thule and Nord in Greenland; Barrow in Alaska, USA; Moosonee in Ontario, Canada; Bravo Ocean Station; Charlie Ocean Station) are depicted in Fig. S2. As documented, during the most intense phase of atmospheric nuclear testing (the 1960s), ^{137}Cs and $^{239+240}$Pu activity concentrations were highest, at several thousand μBq/m^3 and nBq/m^3, respectively (Fig. S2). These contamination levels ceased by the 1980s, once global fallout became negligible, allowing radionuclides from local nuclear emissions and from resuspension to dominate in surface air (Chamizo et al., 2010). For instance, the ^{137}Cs peak noted in 1986 was attributed to post-Chernobyl fallout (Larsen et al. 1989) (Fig. S2). The residual activity concentrations of ^{137}Cs and $^{239+240}$Pu observed in the late 1980s and 1990s were consistent with 21st-century data for suspended aerosols at Hornsund (Fig. S2, Fig. 3 and 4).

3.2 ^{237}Np incidents

The chemical protocol applied in this study was founded on the premise that neptunium occurs at levels below the detection limits of alpha spectrometry for the majority of environmental samples. As estimated by Kelley et al. (1999), deposited activity of ^{237}Np ($T_{1/2}$ = 2.144 10^6 years) is approximately three orders of magnitude lower than that of ^{239}Pu for global fallout. Analyses of three collective samples from Hornsund unexpectedly revealed a distinct ^{237}Np peak that partially overlapped with the ^{242}Pu peak, as shown in Fig. S3. Along with plutonium elution, neptunium is removed from the resin bed; however, no issues are usually encountered during subsequent measurements. This research found ^{237}Np signals in the 2nd half of 2013, the 1st quarter of 2014 and the 4th quarter of 2018. Overlapping spectral lines were resolved by fitting bigaussian curves, allowing count integration (Fig. S3). Unfortunately, the calculation of ^{237}Np activity concentrations was not possible because no neptunium tracer was used during the radiochemical procedure. Pu + Np analytes were successfully separated by approach, unequivocally confirming the presence of ^{237}Np in suspected samples, as exemplified in Fig. S4. The ^{237}Np signal in the 4th quarter of 2018 coincided with a ^{238}Pu outlier.

Detection of ^{237}Np was not reported by other researchers in recent aerosol investigations that employed similar radiochemical procedures without separating plutonium and neptunium fractions (Lujaniene et al., 2012; Nalichowska et al., 2023). This prompted us to conduct in-depth analyses of the blanks, controlling not only the reagents used but also the filter material and equipment in direct contact with the examined samples. The first type of blank comprised only procedural reagents (designated 'blank'), while the second was a simulated collective sample consisting of 12 cleanly pressed Petrianov filters (designated 'blank filter'). It was concluded that the presence of radioisotopes in aerosol samples from Hornsund was not due to laboratory contamination or contamination of a spectrometric unit (Table S2). Further quality control was performed on the reference materials IAEA-447 and IAEA-385 to determine the activity concentrations of the target radionuclides ^{238}Pu, $^{239+240}$Pu and ^{241}Am. The calculated values aligned with the certified values (Table S3).

3.3 Correlation and seasonality evaluation

Spearman's correlation coefficient was selected to minimise the influence of outliers and to account for the non-normal distribution of the data on radioactivity in Hornsund air (Mukaka, 2012; Schober and Schwarte, 2018) (Fig. 5). The correlation outcomes are summarised in Tables 2, 3 and 4. Statistically significant items ($p \leq 0.05$) are indicated by asterisks (*). Additionally, moderate and strong relationships between variables ($|R| \geq 0.4$) are denoted in bold. The input database used to compute the correlation matrix is provided in Tables S4 and S5.

Mutual correlations were at least moderate or strong for ^{7}Be, ^{210}Pb vs air temperature, sum of precipitation, relative humidity, cloudiness, E and NE winds; the latter only for ^{210}Pb (Table 2). Negative monotonic relationships appeared between ^{7}Be, ^{210}Pb and air temperature, sum of precipitation, relative humidity, cloudiness, whereas positive monotonic relationships occurred for ^{7}Be, ^{210}Pb and E wind as well as for ^{210}Pb and NE wind. Moreover, ^{7}Be and ^{210}Pb were not affected by the *SPM* factor (Table 3). These findings corroborated the conclusion concerning the atmospheric transportation and behaviour of ^{7}Be and ^{210}Pb, which were blown into Hornsund by prevailing easterly winds and scavenged by precipitation. Interestingly, quarterly resolution proved adequate for identifying correlations among climatic factors and natural radioisotopes. The ^{137}Cs case appears highly questionable at this point, given that the large number of weekly filters have not contained ^{137}Cs levels above the detection limit since 2013 (Table S5). Artificial radioisotopes exhibited no statistically significant response to climatic conditions, except for $^{239+240}$Pu vs sunshine duration (Table 2). Further evaluation revealed a positive but weak correlation between $^{239+240}$Pu and the *SPM* parameter (Table 3). The dust concentration usually reached a maximum in the 4th quarter (Fig. 2b, Table S5), coinciding with extreme cyclone activity during Arctic winters (Wawrzyniak and Osuch, 2020). Thus, the *SPM* contribution evidenced a partly local origin for $^{239+240}$Pu, likely attributable to dust redistribution in the winter months and to weak soil resuspension in the summer months. This also clarified the weak negative correlation of $^{239+240}$Pu with sunshine duration ($^{239+240}$Pu signals were recorded higher in polar night months than in polar day months).

Strong positive correlations between ^{7}Be and ^{210}Pb were observed annually and in particular quarters (1st, 2nd and 4th) (Table 4). Strong correlations were also noted for $^{239+240}$Pu vs ^{7}Be, $^{239+240}$Pu vs ^{210}Pb and ^{137}Cs vs ^{7}Be in the 1st quarter, and for $^{239+240}$Pu vs ^{241}Am in the 3rd quarter (Table 4). All these relationships were positively monotonic, except for ^{137}Cs vs ^{7}Be. It seems that horizontal air mass movement played a significant role in transporting $^{239+240}$Pu along with ^{7}Be and ^{210}Pb during the 1st quarter. The linkage between ^{241}Am and $^{239+240}$Pu in the 3rd quarter could reflect a similar supply pattern, although this was not easy to define. Moreover, a weak positive correlation of $^{239+240}$Pu vs ^{238}Pu was found annually (Table 4), suggesting that a small portion of ^{238}Pu was likely governed by the natural mechanisms identified for $^{239+240}$Pu. Consistent seasonal fluctuations in the quarterly median values were evident pairwise for ^{7}Be and ^{210}Pb, as well as for $^{239+240}$Pu and ^{238}Pu (Fig. 6). No seasonality could be noticed for ^{137}Cs and ^{241}Am.

Table 2: Mutual correlations between the radioisotope activity concentration and selected meteorological indicators. Statistically significant item ($p \leq 0.05$) is indicated by asterisks (*). Moderate and strong correlation ($|R| \geq 0.4$) is denoted in bold.

	^{7}Be		^{137}Cs		^{210}Pb		$^{239+240}$Pu		^{238}Pu		^{241}Am	
	R	***p***	***R***	***p***	***R***	***p***	***R***	***p***	***R***	***p***	***R***	***p***
Air temperature	**-0.61***	**0.00**	-0.21	0.25	**-0.90***	**0.00**	-0.03	0.84	-0.16	0.29	-0.02	0.92
Sum of precipitation	**-0.47***	**0.00**	-0.27	0.14	**-0.48***	**0.00**	0.18	0.24	-0.03	0.87	-0.11	0.50
Relative humidity	**-0.41***	**0.00**	-0.29	0.11	**-0.75***	**0.00**	0.10	0.52	-0.22	0.16	0.01	0.97
Cloudiness	**-0.52***	**0.00**	-0.09	0.64	**-0.80***	**0.00**	-0.01	0.97	-0.23	0.14	0.00	0.99
Sunshine duration	0.08	0.58	-0.08	0.67	-0.32*	0.01	-0.38*	0.01	-0.20	0.19	0.23	0.13
Visibility	0.10	0.47	-0.16	0.39	-0.12	0.39	-0.20	0.20	0.08	0.63	0.22	0.15
Air pressure	0.01	0.96	-0.17	0.37	-0.23	0.09	-0.27	0.08	0.01	0.94	0.27	0.08
N	0.00	0.97	0.22	0.22	0.11	0.43	0.12	0.43	-0.14	0.38	-	-
NE	0.26	0.06	0.27	0.14	**0.57***	**0.00**	0.30	0.05	0.29	0.06	-0.14	0.37
E	**0.46***	**0.00**	0.21	0.25	**0.55***	**0.00**	0.25	0.10	0.29	0.06	-0.03	0.83
SE	-0.16	0.25	0.19	0.31	-0.28*	0.03	-0.08	0.60	-0.20	0.20	0.04	0.80
S	-0.35*	0.01	-0.23	0.21	-0.35*	0.01	0.10	0.54	-0.17	0.27	0.11	0.47
SW	-0.08	0.55	-0.15	0.40	-0.13	0.32	-0.13	0.39	-0.17	0.27	-0.11	0.47
W	-0.13	0.33	-0.08	0.68	-0.15	0.27	-0.16	0.31	-0.18	0.26	-0.16	0.31
NW	0.22	0.12	-0.11	0.57	0.18	0.19	-0.13	0.41	-0.13	0.39	0.11	0.49

*~~$p \leq 0.05$~~

Table 3: Mutual correlations between the radioisotope activity concentration and *SPM*. Statistically significant item ($p \leq 0.05$) is indicated by asterisks (*). Moderate and strong correlation ($|R| \geq 0.4$) is denoted in bold.

	***SPM* concentration**	
	R	***p***
$^{239+240}$Pu	0.32*	0.04
^{238}Pu	0.23	0.13
^{241}Am	-0.05	0.73
^{7}Be	0.06	0.67
^{137}Cs	0.05	0.77
^{210}Pb	0.23	0.08

*~~$p \leq 0.05$~~

Table 4: Total and seasonal cross-correlations among ^{7}Be, ^{210}Pb, ^{137}Cs, ^{238}Pu, $^{239+240}$Pu and ^{241}Am. Statistically significant item ($p \leq 0.05$) is indicated by asterisks (*). Moderate and strong correlation ($|R| \geq 0.4$) is denoted in bold.

total	**^{238}Pu**		**^{241}Am**		**^{7}Be**		**^{137}Cs**		**^{210}Pb**	
	R	***p***	***R***	***p***	***R***	***p***	***R***	***p***	***R***	***p***
$^{239+240}$Pu	0.33*	0.04	0.20	0.21	-0.21	0.19	-0.19	0.41	-0.08	0.63
^{238}Pu	1.00		0.05	0.76	0.13	0.42	0.10	0.64	0.08	0.59
^{241}Am			1.00		-0.01	0.95	0.05	0.84	0.05	0.71
^{7}Be					1.00		0.20	0.30	**0.78***	**0.00**
^{137}Cs							1.00		0.25	0.17
1st quarter	**^{238}Pu**		**^{241}Am**		**^{7}Be**		**^{137}Cs**		**^{210}Pb**	
	R	***p***	***R***	***p***	***R***	***p***	***R***	***p***	***R***	***p***
$^{239+240}$Pu	0.01	0.99	0.32	0.41	**0.62***	**0.04**	-0.60	0.21	**0.72***	**0.01**
^{238}Pu	1.00		0.16	0.65	0.06	0.85	0.14	0.76	0.07	0.83
^{241}Am			1.00		0.39	0.26	-0.37	0.47	0.39	0.26
^{7}Be					1.00		**-0.78***	**0.01**	**0.56***	**0.04**
^{137}Cs							1.00		-0.29	0.44
2nd quarter	**^{238}Pu**		**^{241}Am**		**^{7}Be**		**^{137}Cs**		**^{210}Pb**	
	R	***p***	***R***	***p***	***R***	***p***	***R***	***p***	***R***	***p***
$^{239+240}$Pu	0.37	0.24	0.14	0.66	0.22	0.5	-0.20	0.80	-0.08	0.81
^{238}Pu	1.00		0.29	0.37	-0.01	0.97	-0.40	0.60	-0.19	0.56
^{241}Am			1.00		-0.39	0.21	-0.40	0.60	-0.17	0.60
^{7}Be					1.00		-0.50	0.39	**0.67***	**0.01**
^{137}Cs							1.00		-0.60	0.28
3rd quarter	**^{238}Pu**		**^{241}Am**		**^{7}Be**		**^{137}Cs**		**^{210}Pb**	
	R	***p***	***R***	***p***	***R***	***p***	***R***	***p***	***R***	***p***
$^{239+240}$Pu	0.47	0.21	**0.74***	**0.01**	0.37	0.29	0.07	0.88	0.25	0.47
^{238}Pu	1.00		-0.05	0.9	-0.07	0.87	0.37	0.47	-0.32	0.41
^{241}Am			1.00		0.22	0.52	-0.04	0.94	0.52	0.08
^{7}Be					1.00		0.43	0.34	0.45	0.14
^{137}Cs							1.00		0.20	0.58
4th quarter	**^{238}Pu**		**^{241}Am**		**^{7}Be**		**^{137}Cs**		**^{210}Pb**	
	R	***p***	***R***	***p***	***R***	***p***	***R***	***p***	***R***	***p***
$^{239+240}$Pu	-0.05	0.91	0.29	0.49	-0.28	0.46	-0.10	0.87	-0.60	0.09
^{238}Pu	1.00		0.01	0.99	0.53	0.10	-0.21	0.64	-0.21	0.54

^{241}Am			1.00		-0.09	0.80	0.66	0.16	-0.07	0.85
^{7}Be					1.00		0.19	0.65	**0.71***	**0.00**
^{137}Cs							1.00		0.62	0.10

* ~~$p \leq 0.05$~~

460

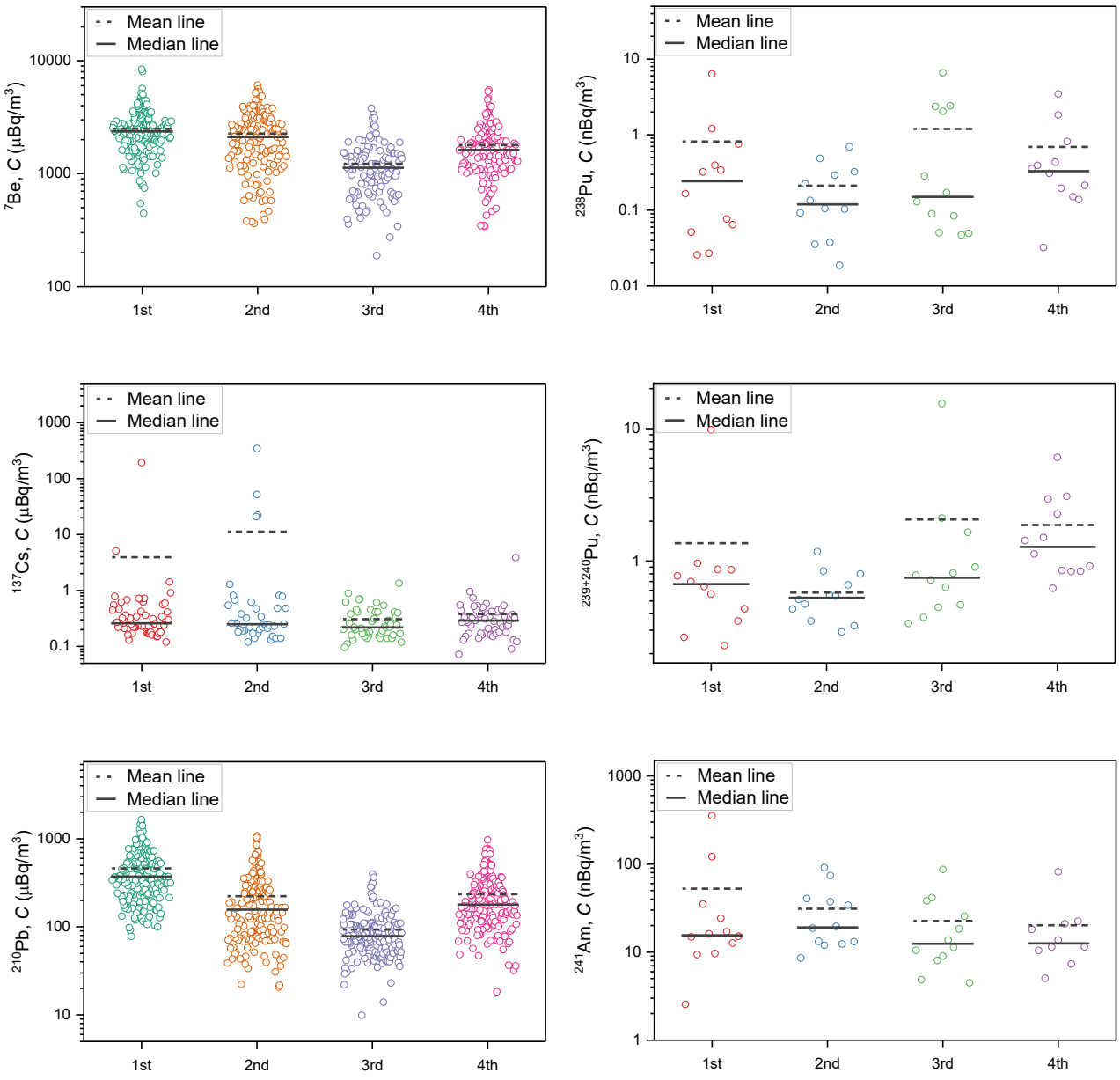

Figure 6: Descriptive statistics for quarters (1st, 2nd, 3rd, 4th) of ^{7}Be, ^{137}Cs, ^{210}Pb, ^{238}Pu, $^{239+240}$Pu and ^{241}Am activity concentrations (*C*) in aerosol samples collected at Hornsund between 2007 and 2021.

3.4 Potential origin of radioactive contamination

The activity ratios (*IR*) of artificial actinides were investigated to infer their provenance (Table S7, Fig. 7), taking into account reference signatures for specific nuclear events provided in Table S6. These ratios are known to vary with reactor type, neutron flux and energy, nuclear fuel burn-up time, or, for fallout from nuclear detonations, bomb type and yield (Oughton et al., 2001). Typically, $^{238}Pu/^{239+240}Pu$ and $^{241}Am/^{239+240}Pu$ ratios in nuclear reactors (NPP) and fuel reprocessing plants (NRP) are about an order of magnitude higher than those for global fallout (GF) or isotopic production grade (PPP) (Table S6).

The $^{238}Pu/^{239+240}Pu$ values ranged from 0.021 to 8.3, whereas the $^{241}Am/^{239+240}Pu$ values varied from 1.5 to 460 in Hornsund air (Table S7). Noteworthy, both maxima were observed in the 1st quarter of 2019. The $^{238}Pu/^{239+240}Pu$ ratios exhibited significant variability throughout 2007–2021, fluctuating predominantly between the reference limits characteristic for GF (+ SNAP 9A) and Chernobyl fallout (Fig. 7). These results pointed to a mixed plutonium origin, affected by both GF (+ SNAP 9A) and releases from nuclear power plants or nuclear reprocessing plants. Moreover, only one point corresponded to the GF (+ SNAP 9A) level, while several points in 2009–2013 and 2017–2020 showed $^{238}Pu/^{239+240}Pu$ ratios noticeably above the known reference signatures (Fig. 7). The latter problem persisted in the $^{241}Am/^{239+240}Pu$ data, demonstrating an unprecedented enhancement of ^{241}Am relative to established activity ratios for prior nuclear events (Fig. 7, Table S7).

Radioactive contamination of the Arctic has occurred at two different scales (AMAP, 2002, 2009):

(a) widespread contamination associated with global nuclear weapons testing (88 of which took place at the Arctic test site of Novaya Zemlya), Sellafield and Cap La Hague releases, and the Chernobyl or Fukushima failures,

(b) localized contamination of smaller areas, for instance, from the bomber crash in Thule and from radioactive waste dumped at sea near Novaya Zemlya (e.g. Abrosimov Fjord, Stepovogo Fjord).

The presence of plutonium and americium fallout from nuclear weapon tests has been well documented in the Spitsbergen region, whereas no such influence has been evidenced following the Chernobyl, Fukushima or Thule accidents (Eriksson et al., 2004; Gwynn et al., 2004; Łokas et al., 2013, 2017b). Nevertheless, elevated $^{238}Pu/^{239+240}Pu$ ratios for cryoconite collected in 2011 from Hans Glaciers on the northern coast of Hornsund indicated a likely contribution from plutonium sources other than global fallout (Łokas et al., 2016). The highest recorded value of $^{238}Pu/^{239+240}Pu$ was 0.118 ± 0.017. Additionally, the $^{241}Am/^{239+240}Pu$ ratios were determined for soils and lake sediments in central Spitsbergen, as well as for proglacial and tundra soils from southwestern Spitsbergen, collected in 2007 and 2005, respectively (Łokas et al., 2017b, a). The results varied from 0.18 to 1.05 in soils and sediments, and from 0.18 to 0.88 in proglacial soils, with maximum values well above the GF level. Although soil, sediment, or cryoconite samples are widely regarded as key environmental matrices in airborne radioactivity investigations, they differ substantially from air filter samples. The former register average contamination accumulated over several years, whereas the latter provide information on airborne pollutants at relatively short intervals (day, week, quarter). Elements of the natural environment exposed to atmospheric fallout over decades are strongly contaminated with a signal from nuclear weapons testing, limiting the ability to detect traces of minor radioactive episodes.

A recent study of air filter samples suggested a mixed origin for plutonium isotopes in Poland and revealed the highest $^{238}Pu/^{239+240}Pu$ ratios of 33.7 ± 3.6 in the 1st quarter of 2000 for Bialystok and 1.29 ± 0.25 in the 1st quarter of 2002 for Krakow (Kierepko et al., 2016; Nalichowska et al., 2023). The $^{238}Pu/^{239+240}Pu$ values determined in aerosol samples collected in Vilnius over the years 2005−2006 varied from 0.028 to 0.042, whereas $^{241}Am/^{239+240}Pu$ values fell within the range of 0.19−0.65, both consistent with the GF (+ SNAP 9A) references. However, a $^{238}Pu/^{239+240}Pu$ level as high as 1.2 ± 0.1 was detected in Lithuanian air in March−April of 2011 (Lujaniene et al., 2012). Findings from surface air in Hornsund during 2007−2021 showed deviations similar to those of $^{238}Pu/^{239+240}Pu$ in Bialystok, Krakow and Vilnius, but not to $^{241}Am/^{239+240}Pu$ in Vilnius.

The provenance of airborne ^{238}Pu enrichment in the European atmosphere has been widely discussed but remains unclear. The following rationale, proposed by researchers, may also shed further light on Hornsund's situation. Potential sources of plutonium in recently measured aerosol samples have been hypothesised to include fuel particles from the Chernobyl or Fukushima accidents and emissions from nuclear installations (i.e. nuclear power plants, nuclear research centres or nuclear fuel reprocessing plants) (Wershofen and Arnold, 1998). Hirose and Povinec (2015) proposed global desert dust events, biomass burning, and sea spray as additional likely delivery patterns. Saharan and Asian dust transport has been classified as the most significant mechanism redistributing aerosols worldwide in the mid-latitude region. The Saharan dust, however, is characterised by isotope ratios typical of global fallout (Chamizo et al., 2010). The Chernobyl ecosystem was affected by several major wildfires, notably in 1992, 1999, 2000, 2002−2004, 2006, 2010, 2015, 2016, 2018 and 2020 (Masson et al., 2021). The dispersion of fly ash particles from biomass combustion has been demonstrated to extend over vast distances, both horizontally (up to several thousand kilometres) and vertically (several kilometres), capable of penetrating the tropopause and reaching the lower stratosphere (Hirose and Povinec, 2015). The contribution of plutonium from sea salt to atmospheric plutonium deposition has been found negligible when compared to soil's (less than 0.3%) (Hirose et al., 2003). The maximum calculated input of sea-spray plutonium to the atmosphere did not exceed 0.006 nBq/m^3, which is by 2–3 orders of magnitude less than that of other plutonium 'feeder' mechanisms.

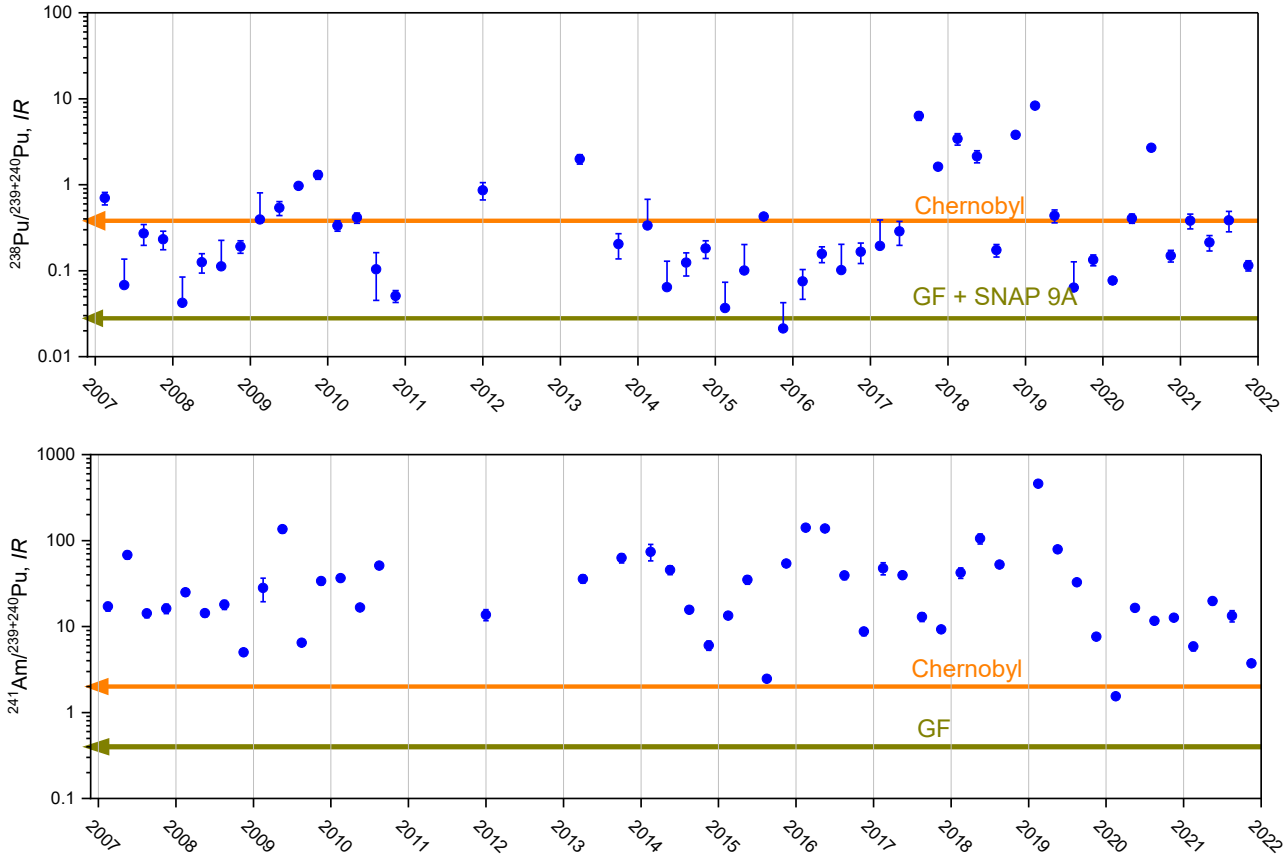

Figure 7: Activity ratios (*IR*) of $^{238}Pu/^{239+240}Pu$ and $^{241}Am/^{239+240}Pu$ for quarterly aerosol samples collected in Hornsund from 2007 to 2021 (error bars represent the 1σ level). GF (+ SNAP 9A) and Chernobyl are used as reference values, based on Table S6.

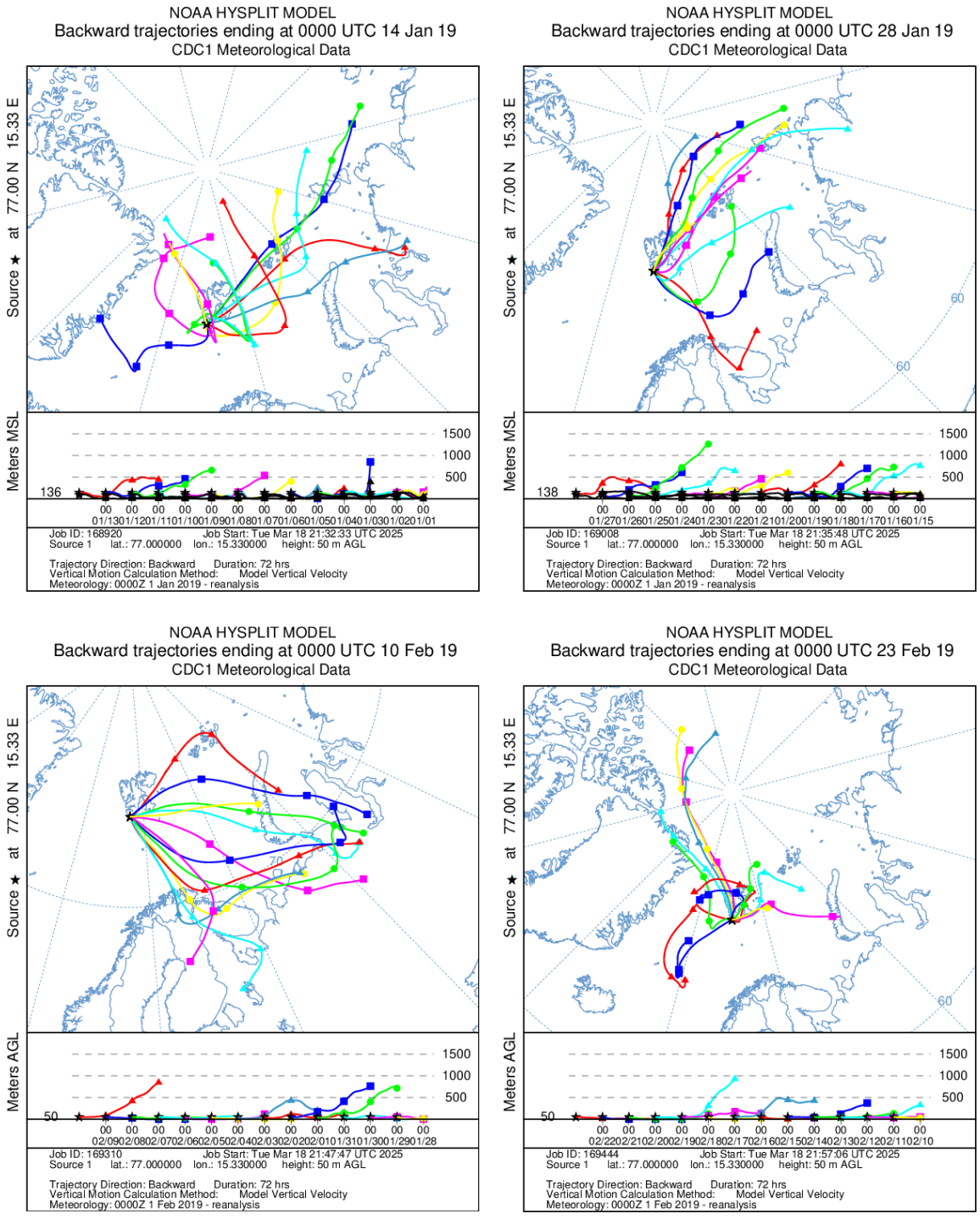

Figure 8: Simulated backward trajectories to the Hornsund study area during the 1st quarter of 2019.

The maximum activity concentration of $^{239+240}$Pu at Hornsund coincided with the highest $^{239+240}$Pu level in Krakow, both noted within the 3rd quarter of 2015. This may have indicated a common source behind the $^{239+240}$Pu peaks; however, the corresponding ^{238}Pu/$^{239+240}$Pu ratios differed. Although the ^{238}Pu/$^{239+240}$Pu result in Krakow could not be attributed to plutonium from spent nuclear fuel, it would explain the situation at Hornsund, as ^{238}Pu/$^{239+240}$Pu and ^{241}Am/$^{239+240}$Pu ratios of 0.426 ± 0.017 and 2.46 ± 0.12, respectively, were consistent with Chernobyl signatures in the period considered (Table S7, Fig. 7). As reported by Evangeliou et al. (2016), about 10.9 TBq of ^{137}Cs, 1.5 TBq of ^{90}Sr, 7.8 GBq of ^{238}Pu, 6.3 GBq of ^{239}Pu, 9.4 GBq of ^{240}Pu and 29.7 GBq of ^{241}Am were released from two major fires in the Chernobyl Exclusion Zone (CEZ) in April and August 2015. The labile elements escaped more easily from the CEZ, whereas the larger refractory particles were removed more efficiently from the atmosphere, affecting mainly the CEZ and its vicinity. During the summer fire, about 75% of the labile and 59% of the refractory radionuclides were exported from the CEZ, with the majority depositing in Belarus and Russia. While the evolution and fate of the plutonium and americium plume modelled by Evangeliou et al. (2016) suggested no spread to Spitsbergen, scheduled measurements of ^{240}Pu/^{239}Pu mass ratios should serve to verify the potential impact of the Chernobyl wildfires on the radioactive signals recorded at Hornsund in 2015. The elevated $^{239+240}$Pu activity concentration in Krakow was likely due to intense resuspension associated with a high number of local fires in Poland that could remobilise the global fallout plutonium present in forest litter (Nalichowska et al., 2023).

The above line of reasoning fails to explain the remarkable enrichment of ^{241}Am between 2007 and 2021, the frequent inputs of ^{238}Pu during 2009–2013 and 2017–2020, or the single ^{237}Np incidents in 2013, 2014 and 2018, detected at the Hornsund station (Fig 7). Correlation and isotopic ratio assessments indicated that a significant proportion of the ^{238}Pu, ^{237}Np and ^{241}Am must have been introduced into the atmosphere via non-natural processes. Identifying the exclusive nuclear emissions of ^{238}Pu, ^{241}Am, and/or ^{237}Np is challenging due to the low time resolution of quarterly filters and the scarcity of data on artificial actinides from other stations in the years explored.

^{238}Pu is characterised by sufficient decay heat to power a deep-space satellite or a space probe via a radioisotope thermoelectric generator (RTG). The well-documented source of ^{238}Pu alone is the SNAP 9A high-atmospheric burn-up in 1964 (Krey, 1967). It is doubtful, however, that ^{238}Pu from the SNAP 9A accident has been present in the stratosphere over the last few decades (Hirose and Povinec, 2015). Since the early 2010s, the US government has initiated efforts to restart the production of ^{238}Pu heat-source material for NASA deep-space missions (Urban-Klaehn et al., 2021; Zillmer et al., 2022). The process involves irradiating a ^{237}Np target with neutrons, converting a portion of ^{237}Np into ^{238}Pu. New production relies on reactors at both Oak Ridge National Laboratory (ORNL) and Idaho National Laboratory (INL). This recent operation has not been associated with reported releases of either ^{238}Pu or ^{237}Np. Radioactive ^{241}Am is commonly used in commercial applications, such as precision measuring devices and smoke detectors. The ^{241}Am activity in various smoke detector models ranged from 7.4 to 740 kBq, distributed under the class exemption (NUREG-1717, 2001; NUREG/CP-0001, 1978; OECD, 1977). The estimated total number of smoke detectors currently in use for residential purposes in the USA is approximately 100 million, with a total ^{241}Am activity of 12 TBq. The high cost of legal storage for spent devices, coupled with homeowners' lack of awareness, has led to disposal with regular waste or common e-waste without any controls. The processing of electrical waste, particularly

isotopic smoke detectors, has been postulated to account for the ^{241}Am release in 2021 over central Poland (Długosz-Lisiecka and Isajenko, 2024). The recycling of these devices with general waste or their combustion at an incineration plant is becoming increasingly popular every year. Importantly, ^{241}Am may also be a generator of ^{237}Np, as the latter is a decay product of ^{241}Am. Recent nuclear episodes provide a new perspective for radioecological research. The presence of ^{106}Ru in European air during autumn 2017 could be attributed to an accident at the Mayak nuclear fuel reprocessing facility during the separation of large quantities of ^{106}Ru from spent nuclear fuel rods. However, alternative explanations include the development of a nuclear engine to power a small missile or drone (Mietelski and Povinec, 2020). Given that the incident followed a nuclear operation that was not formally declared, the exact scenario for large-scale airborne radioactive contamination remains unclear. The Nyonoksa accident in August 2019 (which aligns with official statements about the development of new nuclear-powered missiles in the Russian Federation) could have occurred during preparations for tests of a nuclear engine driven by either a liquid radioisotope generator ^{42}Ar/^{42}K or a small nuclear reactor (Mietelski and Povinec, 2020). There are as yet no reports of possible radioactive leakage into the atmosphere after Nyonoksa. The episodes listed above are indicative of undeclared nuclear activities. The purpose and type of the radioisotopes used are unknown.

A series of transport simulations of nuclear aerosols through the troposphere was performed by the HYSPLIT model, focusing exclusively on the 1st quarter of 2019. During this period, the highest activity concentration among the examined artificial actinides was obtained for ^{241}Am. The dispersion of $^{241}AmO_2$ was investigated over a 72-hour period, with aerosols propagating to altitudes of up to 1 km. Trajectory modelling was initiated on January 1st and continued until March 31st, as depicted in Fig. 8 and Fig. S5. The most noteworthy transport pathways from northern Europe and Asia via the island of Novaya Zemlya were observed between January and February (Fig. 8). Nuclear aerosols were carried at low altitudes in the troposphere (below 100 m), leading to weak dilution and intense deposition. Forward trajectories obtained in early February 2019 indicated significant material shifts from the Novaya Zemlya region to the aerosol sampling point (Fig. S5). Simulations in early January, late February and March demonstrated the presence of additional backward trajectories derived from northern directions (Fig. S5), which seemed unlikely to transport nuclear aerosols highly enriched in ^{241}Am (or other artificial radioisotopes). Reconstructions of aerosol propagation for the remaining period under study, with lower radioisotope activity concentrations than in the 1st quarter of 2019, were beyond the scope of this paper, but are planned to be continued in upcoming scientific exercises.

Conclusions

The present study focused on the Arctic troposphere, providing an experimental aerosol database that has improved considerably since 1999. The activity concentrations of ^{238}Pu, $^{239+240}$Pu and ^{241}Am were determined in the surface air of Hornsund for the years 2007–2021. While the general levels of ^{238}Pu and $^{239+240}$Pu were comparable to recent observations from different sites, ^{241}Am was found to be extraordinarily high, with a maximum of 354 nBq/m^3 detected in the 1st quarter of

2019. Subsequent analysis of isotopic ratios revealed frequent enrichment of ^{238}Pu relative to $^{239+240}$Pu, inconsistent with previously documented releases. Additionally, unexpected single incidents of ^{237}Np were encountered in 2013, 2014 and 2018. A multivariate analysis, incorporating data on ^{7}Be, ^{210}Pb, and ^{137}Cs activity concentrations alongside a wide range of meteorological factors, was applied to explain the behaviour of artificial actinides in the lower atmosphere. Evaluation of Spearman correlations revealed links between the seasonal trends of $^{239+240}$Pu and natural processes, including local redistribution in winter months and horizontal tropospheric transport of haze layers from remote areas in the 1st quarter. Similar mechanisms controlled a proportion of ^{238}Pu, but to a lesser extent. Maximum activity concentrations of 6.61 nBq/m^3 for ^{238}Pu and 15.51 nBq/m^3 for $^{239+240}$Pu were recorded at Hornsund during the 3rd quarter of 2015. Although these peaks coincided with the resuspension and atmospheric transport of radionuclides triggered by 2015 wildfires near the Chornobyl zone, the plume's arrival in the Arctic remains uncertain.

A majority of the significantly elevated levels of ^{241}Am, ^{238}Pu and ^{237}Np were not of natural origin. The average annual doses associated with exposure to suspended artificial actinides were negligible, about 1,000 times lower than the typical background radiation dose of 2.4 mSv per year. Therefore, the detected contamination did not pose a radiological threat to the Arctic environment. Nevertheless, the ^{241}Am, ^{238}Pu, and ^{237}Np signals were alarming, as their occurrence could indicate man-made emissions that were overlooked during the regular monitoring of gamma emitters in Hornsund air. Trajectory simulations for the 1st quarter of 2019 showed the most prominent transport pathways from northern Asia and Europe via the island of Novaya Zemlya. Nuclear aerosols were carried at low altitudes in the troposphere (below 100 m), leading to weak dilution and intense deposition. The research highlighted the importance of including alpha emitters in routine measurements within radiation situation control programmes.

Data availability

Data are available via the Repository of the Institute of Nuclear Physics PAN at https://doi.org/10.48733/no6.25.015.

Author contribution

AC: Writing - original draft, Methodology, Investigation, Formal analysis, Data curation, Conceptualisation, Funding acquisition. AB: Methodology, Investigation, Writing - original draft, Formal analysis. EN: Writing - original draft, Data curation, Formal analysis, Visualisation, Software. MK: Writing - original draft, Resources, Investigation. MD-L: Writing - original draft, Data curation, Formal analysis, Visualisation, Writing - original draft. TW: Writing - original draft, Data curation. EŁ: Resources, Writing - original draft. MG: Visualisation. GL: Investigation.

Competing interests

The authors declare that they have no conflict of interest.

Acknowledgements

The authors acknowledge Katarzyna Barnuś, Mikołaj Wielgat and Michał Palwal for their help during laboratory work.

Financial support

The study was conducted at the Stanisław Siedlecki Polish Polar Station in Hornsund, utilising the infrastructure of the Institute of Geophysics of the Polish Academy of Sciences. It was funded by the Polish Ministry of Science and Higher Education and contributed to funding actions of the Svalbard Integrated Arctic Earth Observing System (SIOS). The National Science Centre of Poland supported the research component dedicated to alpha-emitter analyses under project No. 2021/43/D/ST10/02049.

References

Aegerter, S., Bhandari, N., Rama Tamhane, and Tamhane, A. S.: 7Be and 32P in ground level air, Tellus, 18, 212–215, https://doi.org/10.3402/tellusa.v18i2-3.9679, 1966.

Alvarado, J. A. C., Steinmann, P., Estier, S., Bochud, F., Haldimann, M., and Froidevaux, P.: Anthropogenic radionuclides in atmospheric air over Switzerland during the last few decades, Nat. Commun., 5, 1–6, https://doi.org/10.1038/ncomms4030, 2014.

AMAP: Radioactivity in the Arctic, Arctic Monitoring and Assessment Programme, Oslo, Norway, 2002.

AMAP: Radioactivity in the Arctic, Arctic Monitoring and Assessment Programme, Oslo, Norway, 2009.

AMAP: Radioactivity in the Arctic, Arctic Monitoring and Assessment Programme, Oslo, Norway, 2015.

Baré, J., Gheddou, A., and Kalinowski, M. B.: Overview of temporary radioxenon background measurement campaigns conducted for the CTBTO between 2008 and 2018, J. Environ. Radioact., 257, https://doi.org/10.1016/j.jenvrad.2022.107053, 2023.

Barrie, L. A., Hoff, R. M., and Daggupaty, S. M.: The influence of mid-latitudinal pollution sources on haze in the Canadian arctic, Atmos. Environ., 15, 1407–1419, https://doi.org/10.1016/0004-6981(81)90347-4, 1981.

Beer, J., McCracken, K., and von Steiger, R.: Cosmogenic Radionuclides - Theory and Applications in the Terrestrial and Space Environments, Springer Berlin Heidelberg, 1689–1699 pp., https://doi.org/10.1017/CBO9781107415324.004, 2019.

Błażej, S. and Mietelski, J. W.: Cosmogenic 22 Na, 7 Be and terrestrial 137 Cs, 40 K radionuclides in ground level air samples collected weekly in Kraków (Poland) over years 2003-2006, J. Radioanal. Nucl. Chem., 300, 747–756, https://doi.org/10.1007/s10967-014-3049-6, 2014.

Bossew, P., Gering, F., Petermann, E., Hamburger, T., Katzlberger, C., Hernandez-Ceballos, M. A., De Cort, M., Gorzkiewicz, K., Kierepko, R., and Mietelski, J. W.: An episode of Ru-106 in air over Europe, September–October 2017 – Geographical distribution of inhalation dose over Europe, J. Environ. Radioact., 205–206, 79–92, https://doi.org/10.1016/j.jenvrad.2019.05.004, 2019.

Burakowska, A., Kubicki, M., Mysłek-Laurikainen, B., Piotrowski, M., Trzaskowska, H., and Sosnowiec, R.: Concentration of 7Be, 210Pb, 40K, 137Cs, 134Cs radionuclides in the ground layer of the atmosphere in the polar (Hornsund, Spitsbergen) and mid-latitudes (Otwock-Świder, Poland) regions, J. Environ. Radioact., 240, https://doi.org/10.1016/j.jenvrad.2021.106739, 2021.

Chamizo, E., García-León, M., Enamorado, S. M., Jiménez-Ramos, M. C., and Wacker, L.: Measurement of plutonium isotopes, 239Pu and 240Pu, in air-filter samples from Seville (2001-2002), Atmos. Environ., 44, 1851–1858, https://doi.org/10.1016/j.atmosenv.2010.02.030, 2010.

Coyne, J., Bobrov, D., Bormann, P., Duran, E., Grenard, P., Haralabus, G., Kitov, I., and Starovoit, Y.: CTBTO: Goals, networks, data analysis and data availability, in: New manual of seismological observatory practice 2 (NMSOP-2), Deutsches GeoForschungsZentrum GFZ, 1–41, https://doi.org/10.2312/GFZ.NMSOP-2, 2012.

Currie, L. A.: Limits for Qualitative Detection and Quantitative Determination: Application to Radiochemistry, Anal. Chem., 40, 586–593, https://doi.org/10.1021/ac60259a007, 1968.

Długosz-Lisiecka, M. and Isajenko, K.: Am-241 in the urban air – Monitoring and simulation results, Process Safety and Environmental Protection, 186, 639–644, https://doi.org/10.1016/j.psep.2024.03.124, 2024.

Dueñas, C., Fernández, M. C., Carretero, J., Liger, E., and Cañete, S.: Atmospheric deposition of 7Be at a coastal Mediterranean station, Journal of Geophysical Research Atmospheres, 106, 34059–34065, https://doi.org/10.1029/2001JD000771, 2001.

Engelbrecht, R. and Schwaiger, M.: State of the art of standard methods used for environmental radioactivity monitoring, Applied Radiation and Isotopes, 66, 1604–1610, https://doi.org/10.1016/j.apradiso.2008.01.021, 2008.

Eriksson, M., Holm, E., Roos, P., and Dahlgaard, H.: Distribution and flux of 238Pu, 239,240Pu, 241Am, 137Cs and 210Pb to high arctic lakes in the Thule district (Greenland), J. Environ. Radioact., 75, 285–299, https://doi.org/10.1016/j.jenvrad.2003.12.007, 2004.

Evangeliou, N., Zibtsev, S., Myroniuk, V., Zhurba, M., Hamburger, T., Stohl, A., Balkanski, Y., Paugam, R., Mousseau, T. A., Møller, A. P., and Kireev, S. I.: Resuspension and atmospheric transport of radionuclides due to wildfires near the Chernobyl Nuclear Power Plant in 2015: An impact assessment, Sci. Rep., 6, https://doi.org/10.1038/srep26062, 2016.

Feely, H. W., Helfer, I. K., Juzdan, Z. R., Klusek, C. S., Larsen, R. J., Leifer, R., Sanderson, C. G., and Dreicer, M.: Fallout in the New York metropolitan area following the chernobyl accident, J. Environ. Radioact., 7, 177–191, https://doi.org/10.1016/0265-931X(88)90006-9, 1988.

Feely, H. W., Larsen, R. J., and Sanderson, C. G.: Factors that cause seasonal variations in Beryllium-7 concentrations in surface air, J. Environ. Radioact., 9, 223–249, https://doi.org/10.1016/0265-931X(89)90046-5, 1989.

Furuno, A., Ohmori, R., Tateoka, H., Minakawa, Y., Kurihara, T., Yamamoto, Y., and Tomita, Y.: Assessment of Caesium-137 Detections at CTBTO Radionuclide Monitoring Stations in East Asia and Their Relationship to Asian Dust Dispersion, Pure Appl. Geophys., https://doi.org/10.1007/s00024-024-03620-y, 2024.

Gäggeler, H. W.: Radioactivity in the Atmosphere, Ract, 70–71, 345–354, https://doi.org/10.1524/ract.1995.7071.special-issue.345, 1995.

Gorzkiewicz, K., Kierepko, R., Paatero, J., Virkkula, A., and Mietelski, J. W.: Air radioactivity in Marambio Base: The peculiar character of Antarctic Peninsula, J. Environ. Radioact., 251–252, 106930, https://doi.org/10.1016/j.jenvrad.2022.106930, 2022.

Grossi, C., Ballester, J., Serrano, I., Galmarini, S., Camacho, A., Curcoll, R., Morguí, J. A., Rodò, X., and Duch, M. A.: Influence of long-range atmospheric transport pathways and climate teleconnection patterns on the variability of surface 210Pb and 7Be concentrations in southwestern Europe, J. Environ. Radioact., 165, 103–114, https://doi.org/10.1016/j.jenvrad.2016.09.011, 2016.

Gwynn, J. P., Dowdall, M., Davids, C., Selnæs, Ø. G., and Lind, B.: The radiological environment of Svalbard, Polar Res., 23, 167–180, https://doi.org/10.1111/j.1751-8369.2004.tb00006.x, 2004.

Hirose, K. and Povinec, P. P.: Sources of plutonium in the atmosphere and stratosphere-troposphere mixing, Sci. Rep., 5, 1–9, https://doi.org/10.1038/srep15707, 2015.

Hirose, K., Igarashi, Y., Aoyama, M., Kim, C. K., Kim, C. S., and Chang, B. W.: Recent trends of plutonium fallout observed in Japan: Plutonium as a proxy for desertification, Journal of Environmental Monitoring, 5, 302–307, https://doi.org/10.1039/b212560a, 2003.

Hoover, M. D. and Maiello, M. L.: Radioactive Air Sampling Methods, CRC Press Taylor & Francis Group, Boca Raton London New York, 1–581 pp., https://doi.org/10.1097/hp.0b013e318217066b, 2010.

ICRP: 1990 Recommendations of the International Commission on Radiological Protection. ICRP Publication 60, Ann. ICRP, 21, 1991.

ICRP: The 2007 Recommendations of the International Commission on Radiological Protection. ICRP Publication 103, Ann. ICRP, 37, 2007.

IPCC: IPCC Special Report on the Ocean and Cryosphere in a Changing Climate, edited by: Pörtner, H.-O., Roberts, D. C., Masson-Delmotte, V., Zhai, P., Tignor, M., Poloczanska, E., Mintenbeck, K., Alegría, A., Nicolai, M., Okem, A., Petzold, J., Rama, B., and Weyer, N. M., Cambridge University Press, Cambridge, UK and New York, NY, USA, https://doi.org/10.1017/CBO9781139177245.003, 2019.

Kelley, J. M., Bond, L. A., and Beasley, T. M.: Global distribution of Pu isotopes and 237Np, Science of the Total Environment, 237–238, 483–500, https://doi.org/10.1016/S0048-9697(99)00160-6, 1999.

Kierepko, R., Mietelski, J. W., Ustrnul, Z., Anczkiewicz, R., Wershofen, H., Holgye, Z., Kapała, J., and Isajenko, K.: Plutonium isotopes in the atmosphere of Central Europe: Isotopic composition and time evolution vs. circulation factors, Science of the Total Environment, 569–570, 937–947, https://doi.org/10.1016/j.scitotenv.2016.05.222, 2016.

Koo, Y. H., Yang, Y. S., and Song, K. W.: Radioactivity release from the Fukushima accident and its consequences: A review, Progress in Nuclear Energy, 74, 61–70, https://doi.org/10.1016/j.pnucene.2014.02.013, 2014.

Krey, P. W.: Atmospheric burnup of a plutonium-238 generator, Science (1979)., 158, 769–771, https://doi.org/10.1126/science.158.3802.769, 1967.

Kulan, A., Aldahan, A., Possnert, G., and Vintersved, I.: Distribution of 7Be in surface air of Europe, Atmos. Environ., 40, 3855–3868, https://doi.org/10.1016/j.atmosenv.2006.02.030, 2006.

Larsen, R. J.: Letter To The Editor: Global Decrease of Beryllium in Surface Air, J. Environ. Radioact., 18, 85–87, https://doi.org/10.1080/13518040701205365, 1993.

Larsen, R. J.: Letter To The Editor: Fission Products Detected in Alaska Following the Tomsk-7 Accident, Int. J. Phytoremediation, 23, 205–209, https://doi.org/10.1080/13518040701205365, 1994.

Larsen, R. J., Haagenson, P. L., and Reiss, N. M.: Transport processes associated with the initial elevated concentrations of Chernobyl radioactivity in surface air in the United States, J. Environ. Radioact., 10, 1–18, https://doi.org/10.1016/0265-931X(89)90002-7, 1989.

Larsen, R. J., Sanderson, C. G., and Kada, J.: EML Surface Air Sampling Program, 1990-1993 Data, New York, 1995.

Lee, H. N. and Feichter, J.: An intercomparison of wet precipitation scavenging schemes and the emission rates of 222Rn for the simulation of global transport and deposition of 210Pb, J. Geophys. Res., 100, https://doi.org/10.1029/95jd01732, 1995.

Łokas, E., Mietelski, J. W., Ketterer, M. E., Kleszcz, K., Wachniew, P., Michalska, S., and Miecznik, M.: Sources and vertical distribution of 137Cs, 238Pu, 239+240Pu and 241Am in peat profiles from southwest Spitsbergen, Applied Geochemistry, 28, 100–108, https://doi.org/10.1016/j.apgeochem.2012.10.027, 2013.

Łokas, E., Zaborska, A., Kolicka, M., Różycki, M., and Zawierucha, K.: Accumulation of atmospheric radionuclides and heavy metals in cryoconite holes on an Arctic glacier, Chemosphere, 160, 162–172, https://doi.org/10.1016/j.chemosphere.2016.06.051, 2016.

Łokas, E., Wachniew, P., Jodłowski, P., and Gąsiorek, M.: Airborne radionuclides in the proglacial environment as indicators of sources and transfers of soil material, J. Environ. Radioact., 178–179, 193–202, https://doi.org/10.1016/j.jenvrad.2017.08.018, 2017a.

Łokas, E., Zwoliński, Z., Rachlewicz, G., Gąsiorek, M., Wilkosz, G., and Samolej, K.: Distribution of anthropogenic and naturally occurring radionuclides in soils and lakes of Central Spitsbergen (Arctic), J. Radioanal. Nucl. Chem., 311, 707–717, https://doi.org/10.1007/s10967-016-5085-x, 2017b.

Lujaniene, G., Valiulis, D., Byčenkien, S., Šakalys, J., and Povinec, P. P.: Plutonium isotopes and 241Am in the atmosphere of Lithuania: A comparison of different source terms, Atmos. Environ., 61, 419–427, https://doi.org/10.1016/j.atmosenv.2012.07.046, 2012.

Marsz, A. and Styszyńska, A.: Climate and Climate Change at Hornsund, Svalbard, Gdynia Maritime University, Gdynia, 2013.

Masson, O., Piga, D., Gurriaran, R., and D'Amico, D.: Impact of an exceptional Saharan dust outbreak in France: PM10 and artificial radionuclides concentrations in air and in dust deposit, Atmos. Environ., 44, 2478–2486, https://doi.org/10.1016/j.atmosenv.2010.03.004, 2010.

Masson, O., Romanenko, O., Saunier, O., Kirieiev, S., Protsak, V., Laptev, G., Voitsekhovych, O., Durand, V., Coppin, F., Steinhauser, G., De Vismes Ott, A., Renaud, P., Didier, D., Boulet, B., Morin, M., Hýža, M., Camps, J., Belyaeva, O., Dalheimer, A., Eleftheriadis, K., Gascó-Leonarte, C., Ioannidou, A., Isajenko, K., Karhunen, T., Kastlander, J., Katzlberger, C., Kierepko, R., Knetsch, G. J., Kónyi, J. K., Mietelski, J. W., Mirsch, M., Møller, B., Nikolić, J. K., Rusconi, R., Samsonov, V., Simion, E., Steinmann, P., Stoulos, S., Suarez-Navarro, J. A., Wershofen, H., Zapata-García, D., and Zorko, B.: Europe-Wide Atmospheric Radionuclide Dispersion by Unprecedented Wildfires in the Chernobyl Exclusion Zone, April 2020, Environ. Sci. Technol., 55, 13834–13848, https://doi.org/10.1021/acs.est.1c03314, 2021.

Mietelski, J. W. and Povinec, P. P.: Environmental radioactivity aspects of recent nuclear accidents associated with undeclared nuclear activities and suggestion for new monitoring strategies, J. Environ. Radioact., 214–215, 106151, https://doi.org/10.1016/j.jenvrad.2019.106151, 2020.

Mietelski, J. W., Gaca, P., and Olech, M. A.: Radioactive contamination of lichens and mosses collected in South Shetlands and Antarctic Peninsula, 245, 527–537, 2000.

Mietelski, J. W., Kubica, B., Gaca, P., Tomankiewicz, E., Błażej, S., Tuteja-Krysa, M., and Stobiński, M.: 238 Pu, 239+240 Pu, 241 Am, 90 Sr and 137 Cs in mountain soil samples from the Tatra National Park (Poland), J. Radioanal. Nucl. Chem., 275, 523–533, https://doi.org/10.1007/s10967-007-7026-1, 2008.

Mukaka, M. M.: Correlation coefficient and its use, Malawi Medical Journal, 24, 69–71, 2012.

Nalichowska, E., Mietelski, J. W., Kierepko, R., Ustrnul, Z., Gorzkiewicz, K., Brudecki, K., and Kowalska, A.: Plutonium isotopes in the ground air layer in southern Poland (2010–2016): Source terms, seasonal variability and correlations with meteorological conditions, J. Environ. Radioact., 264, 107204, https://doi.org/10.1016/j.jenvrad.2023.107204, 2023.

NUREG-1717: Systematic Radiological Assessment of Exemptions for Source and Byproduct Materials, U. S. Nuclear Regulatory Commission, 2001.

NUREG/CP-0001: Radioactivity in Consumer Products, U. S. Nuclear Regulatory Commission, 1978.

OECD: Recommendations for ionization chamber smoke detectors in implementation of radiation protection standards, Nuclear Energy Agency, Organisation for Economic Co-operation and Development, 1977.

Oughton, D., Day, P., and Fifield, K.: Plutonium measurement using accelerator mass spectrometry: Methodology and applications, Radioactivity in the Environment, 1, 47–62, https://doi.org/10.1016/S1569-4860(01)80006-1, 2001.

Paatero, J., Hatakka, J., Holmén, K., Eneroth, K., and Viisanen, Y.: Lead-210 concentration in the air at Mt. Zeppelin, Ny-Ålesund, Svalbard, Physics and Chemistry of the Earth, 28, 1175–1180, https://doi.org/10.1016/j.pce.2003.08.050, 2003.

Paatero, J., Buyukay, M., Holmén, K., Hatakka, J., and Viisanen, Y.: Seasonal variation and source areas of airborne lead-210 at Ny-Ålesund in the High Arctic, Polar Res., 29, 345–352, https://doi.org/10.1111/j.1751-8369.2010.00185.x, 2010.

Povinec, P. P., Gera, M., Holý, K., Hirose, K., Lujanienė, G., Nakano, M., Plastino, W., Sýkora, I., Bartok, J., and Gažák, M.: Dispersion of Fukushima radionuclides in the global atmosphere and the ocean, Applied Radiation and Isotopes, 81, 383–392, https://doi.org/10.1016/j.apradiso.2013.03.058, 2013.

Rahn, K. A.: Relative importances of North America and Eurasia as sources of arctic aerosol, Atmospheric Environment (1967), 15, 1447–1455, https://doi.org/10.1016/0004-6981(81)90351-6, 1981.

Rinke, A., Maturilli, M., Graham, R. M., Matthes, H., Handorf, D., Cohen, L., Hudson, S. R., and Moore, J. C.: Extreme cyclone events in the Arctic: Wintertime variability and trends, Environmental Research Letters, 12, https://doi.org/10.1088/1748-9326/aa7def, 2017.

La Rosa, J. J., Cooper, E. L., Ghods-Esphahani, A., Jansta, V., Makarewicz, M., Shawky, S., and Vajda, N.: Radiochemical methods used by the IAEA's laboratories at Seibersdorf for the determination of 90Sr, 144Ce and Pu radionuclides in environmental samples collected for the International Chernobyl project, J. Environ. Radioact., 17, 183–209, https://doi.org/10.1016/0265-931X(92)90025-O, 1992.

La Rosa, J., Gastaud, J., Lagan, L., Lee, S. H., Levy-Palomo, I., Povinec, P. P., and Wyse, E.: Recent developments in the analysis of transuranics (Np, Pu, Am) in seawater, J. Radioanal. Nucl. Chem., 263, 427–436, https://doi.org/10.1007/s10967-005-0072-7, 2005.

Schober, P. and Schwarte, L. A.: Correlation coefficients: Appropriate use and interpretation, Anesth. Analg., 126, 1763–1768, https://doi.org/10.1213/ANE.0000000000002864, 2018.

Stein, A. F., Draxler, R. R., Rolph, G. D., Stunder, B. J. B., Cohen, M. D., and Ngan, F.: Noaa's hysplit atmospheric transport and dispersion modeling system, Bull. Am. Meteorol. Soc., 96, 2059–2077, https://doi.org/10.1175/BAMS-D-14-00110.1, 2015.

Steinhauser, G., Brandl, A., and Johnson, T. E.: Comparison of the Chernobyl and Fukushima nuclear accidents: A review of the environmental impacts, Science of the Total Environment, 470–471, 800–817, https://doi.org/10.1016/j.scitotenv.2013.10.029, 2014.

UNSCEAR: Ionizing Radiation: Sources and Biological Effects; ANNEX E. Exposures Resulting from Nuclear Explosions. Report to General Assembly, United Nations Scientific Committee on the Effects of Atomic Radiation, New York, 1982.

UNSCEAR: Sources and Effects of Ionizing Radiation; ANNEX B. Exposures from Man-made Sources of Radiation. Report to the General Assembly, United Nations, New York, 1993.

UNSCEAR: Sources and Effects of Ionizing Radiation; ANNEX C. Exposures to the Public from Man-made Sources of Radiation. Report to the General Assembly, UNITED NATIONS, New York, 2000a.

UNSCEAR: Sources and Effects of Ionizing Radiation; ANNEX J. Exposure and Effects of Chernobyl Accident. Report to General Assembly, New York, 2000b.

Urban-Klaehn, J., Miller, D., Gross, B. J., Tyler, C. R., and Dwight, C. C.: Initial phase of Pu-238 production in Idaho National Laboratory, Applied Radiation and Isotopes, 169, https://doi.org/10.1016/j.apradiso.2020.109517, 2021.

Wawrzyniak, T. and Osuch, M.: A 40-year High Arctic climatological dataset of the Polish Polar Station Hornsund (SW Spitsbergen, Svalbard), Earth Syst. Sci. Data, 12, 805–815, https://doi.org/10.5194/essd-12-805-2020, 2020.

Wershofen, H. and Arnold, D.: Radionuclides in Ground-level Air in Braunschweig-Report of the PTB Trace Survey Station Physikalisch-Technische Bundesanstalt, 1998.

Zhang, W., Paatero, J., Leppänen, A. P., Møller, B., Jensen, L. K., Gudnason, K., Sofiev, M., Anderson, P., Sickel, M., Burakowska, A., Kubicki, M., and Anderson, A.: Evaluation of 137Cs, 133Xe and 3H activity concentrations monitored in the Arctic atmosphere, J. Environ. Radioact., 253–254, https://doi.org/10.1016/j.jenvrad.2022.107013, 2022.

Zillmer, A., Green, W., Tyler, C., Gross, B., Rosvall, E., Fradeneck, A., Fishler, J., Reeder, D., Marlow, R., Urban-Klaehn, J., Reichenberger, M., Hill, M., and Howard, R.: Recent 238Pu Production Activities at Idaho National Laboratory, Nucl. Technol., 208, S1–S10, https://doi.org/10.1080/00295450.2022.2105774, 2022.